On the Relationship Between Star Formation and the ISM

On the Relationship Between Star Formation and the Interstellar Medium in Numerical Simulations

By

Samantha M. Benincasa, B.Sc.

A Thesis

Submitted to the School of Graduate Studies

in Partial Fulfilment of the Requirements

for the Degree

Master of Science

McMaster University

Master of Science (2014) McMaster University

(Physics and Astronomy) Hamilton, Ontario

TITLE: On the Relationship Between Star Formation and the Interstellar Medium in Numerical Simulations

AUTHOR: Samantha Benincasa, B.Sc. (McMaster University)

SUPERVISOR: James Wadsley, Hugh Couchman

NUMBER OF PAGES: x, 80

Abstract

The cycle of star formation is the key to galaxy evolution. Stars form in massive collections of extremely dense cold gas. Stellar feedback will inject turbulence into the interstellar medium (ISM) and regulate the availability of more star-forming gas. This gas is an integral component in the cycle of star formation but is very difficult to model in numerical simulations. We have investigated the interplay between star formation and the structure of the ISM in numerical simulations. These simulations were done using the Smoothed Particle Hydrodynamics code GASOLINE. For this work we introduce a new treatment for photoelectric heating in GASOLINE. We first explore the impact of numerical parameter choices for the star formation threshold density ($n_{\rm th}$), star formation efficiency (c_*) and feedback efficiency ($\epsilon_{\rm FB}$). Of these three parameters, only the feedback efficiency plays a large role in determining the global star formation rate of the galaxy. Further, we explore the truncation of star formation in the outer regions of galactic discs and its relation to the presence of a two-phase thermal instability. In the outer regions of the simulated discs, gas exists almost exclusively in one warm phase, unsuitable to host large-scale star formation. We find that the disappearance of two-phase structure in the ISM corresponds to the truncation of star formation.

Acknowledgements

Firstly, and most importantly, thank you to my supervisors James Wadsley and Hugh Couchman. To Hugh, for your amazing insight and to James for your constant encouragement and infectious enthusiasm. You must both have a never-ending reserve of patience; when I've needed reassurance you've kindly provided it in spades.

To Elizabeth Tasker thank you more times than I can say. Thank you for giving me the opportunity to visit you in Sapporo, and for accompanying me inside a dimly lit 40 ft. Buddha while I was there. You're constantly in my corner and that knowledge has made all the difference in the world. You helped me realize that I wasn't done yet; I'm holding you responsible for the next four years.

To my office-mates past and present, official and unofficial, you've pulled me through. You ate my stress baking, listened when I needed to talk and joked when I needed to laugh. You've made the last two years so much fun with countless coffee breaks, astro pancakes, softball games and Friday night Dr. Who pizza. In particular, I have to give two special thank you's. To Ben Keller for happily explaining all things SPH to me one million and one times. And of course, to Rachel Ward-Maxwell for all the walks, all the hugs and all the glitter.

To my friends and family, thank you for your unconditional love and support. It has meant more to me than anything else.

to my grandparents

Table of Contents

Descriptive Notes ii

Abstract iii

Acknowledgements iv

List of Figures viii

List of Tables x

Chapter 1 Introduction **1**

1.1 Star Formation 1

1.1.1 Stellar Feedback 5

1.2 The Interstellar Medium 5

1.2.1 Heating and Cooling in the ISM 7

1.3 The Interplay Between Stars and the ISM 8

1.4 Numerical Studies of the ISM 12

1.4.1 The Impacts of Numerical Choices 13

1.5 Overview 14

Chapter 2 Methods **18**

2.1 Smoothed Particle Hydrodynamics 18

2.2 GASOLINE 20

2.2.1 Star Formation 21

2.2.2 Feedback 21

2.2.3 Photoelectric Heating 22

2.3 The Initial Conditions 23

2.3.1 Density Profile 24

2.3.2 Turbulence 25

2.3.3 Evolution 26

2.4 Consequences of the Photoelectric Heating Term 27

Chapter 3 Simulation Results & Discussion **31**

3.1 Simulations 31

3.1.1 Initial Analysis 33

3.2 Star Formation: A Self-Regulating Cycle 45

3.2.1 Density Threshold ($n_{\rm th}$) 45

3.2.2 Star Formation Efficiency (c_*) 52

3.2.3 Supernovae Feedback Efficiency ($\epsilon_{\rm FB}$) 57

3.2.4 A Resolution Study 64

3.3 The Correlation Between Pressure and Star Formation 67

3.3.1 Extended Disc Models 70

Chapter 4 Conclusions & Future Work **78**

List of Figures

1.1 The observed global Kennicutt-Schmidt relation 3

1.2 Equilibrium phase diagram 8

2.1 The smoothing kernel 20

2.2 The surface density profile of the initial conditions 24

2.3 A comparison of the choice of $T_{\rm init}$ 26

2.4 The effect of a radially varying FUV term on ISM 28

3.1 Star formation rates for low surface density discs 36

3.2 Star formation rates for high surface density discs 37

3.3 Phase diagrams for low surface density discs 38

3.4 Phase diagrams for high surface density discs 39

3.5 Gas fractions for high surface density discs 40

3.6 Scale height for high surface density discs 41

3.7 Density slices for low surface density discs 42

3.8 Density slices for high surface density discs 43

3.9 The global Kennicutt-Schmidt relation for our simulated galaxies 44

3.10 The impact of the choice of $n_{\rm th}$ on the SFR 46

3.11 The impact of the choice of $n_{\rm th}$ on the phases of the ISM 48

3.12 Surface density of young stars in simulations with varying $n_{\rm th}$ . . 50

3.13 Age of young stars in simulations with varying $n_{\rm th}$ 51

3.14 The impact of the choice of c_* on the SFR 53

3.15 Density of gas in s14.n100.c0.35 54

3.16 Density of gas in s14.n100.c6 55

3.17 The impact of the choice of c_* on the phases of the ISM 57

3.18 The impact of the choice of $\epsilon_{\rm FB}$ on the SFR 59

3.19 The impact of the choice of $\epsilon_{\rm FB}$ on the phases ISM 61

3.20 Phase diagrams for discs with varying $\epsilon_{\rm FB}$ 62

3.21 Radial pressure for discs with varying $\epsilon_{\rm FB}$ 63

3.22 A resolution study for the simulation s7.n100.c6 - xy Density Slices 65

3.23 A resolution study for the simulation s7.n100.c6 - ISM Properties 66

3.24 Average pressure in a selected low surface density disc 68

3.25 Average pressure in a selected high surface density disc 69

3.26 Density of gas in extended disc s14.n10^4.c5.lowFB.x 71

3.27 Density of gas in extended disc s14.n10^4.c5.lowFB.x.FUVR$_0$ . . . 72

3.28 Average pressure for the fiducial extended disc 73

3.29 Average pressure for the extended disc with modified FUV heating 74

List of Tables

1.1 The Phase Structure of the ISM 6

3.1 List of Simulations 32

Chapter 1

Introduction

Galaxies are the star formation engines of the universe. Our own galaxy, the Milky Way, forms stars at a rate of 2-4 $M_\odot$ yr^{-1}, a modest rate (Kennicutt & Evans, 2012, and references therein). Elsewhere in the universe live a zoo of other types of galaxies, for example Starburst galaxies generating enormous amounts of stars at rates as high as 1000 $M_\odot$ yr^{-1} (Solomon & Vanden Bout, 2005). It is the interplay between stars and the Interstellar Medium (ISM) that shapes the structure and properties of galaxies, particularly how efficiently stars are made. Recent large-scale observational surveys, like The HI Nearby Galaxies Survey (THINGS) have provided us with a look at galaxies and star formation on sub-kpc scales (Walter et al., 2008). There are many complex processes involved in the ISM, including star formation, gas heating and cooling and stellar feedback as described below.

1.1 Star Formation

In the local universe stars form exclusively in dense clouds of dust and molecular hydrogen gas within galaxies. Collectively, these clouds are referred

to as Giant Molecular Clouds (GMCs) and have average densities of 100 cm^{-3} and masses above 10^4 $M_\odot$ (Tielens, 2005). While these objects contain the fuel for star formation, this fuel will not be entirely consumed. We can define a depletion time, τ_{dep}, defined as the timescale required to consume the available molecular hydrogen reservoir at the current star formation rate. When averaged over kpc scales, this timescale is thought to fall between $1 - 2$ Gyr (Leroy et al., 2013). In typical galaxies the conversion of GMC gas into stars is thought to be extremely inefficient, with only 1-2% of gas actually becoming stars (Krumholz & Tan, 2007).

Although the process is inefficient, stars will eventually condense out of molecular clumps and cores, even denser substructures within GMCs (McKee & Ostriker, 2007). Star formation proceeds in cores where the average density has surpassed 10^4 cm^{-3} (Lada et al., 2010).

The rate of star formation correlates strongly with gas density, specifically that of molecular hydrogen (H_2). For entire galaxies, this correlation emerges in the form of the Kennicutt-Schmidt relation (Schmidt, 1959; Kennicutt, 1998). This relation correlates star formation rate surface density ($\Sigma_{\rm SFR}$) with gas surface density ($\Sigma_{\rm gas}$):

$$\Sigma_{\rm SFR} = {\rm A}\Sigma_{\rm gas}^{\rm N} \tag{1.1}$$

where typically A$= 2.5 \times 10^{-4}$ $M_\odot$ kpc^{-2} yr^{-1} and the power-law slope is N$= 1.4$ (Kennicutt, 1998). The global Kennicutt-Schmidt relation is shown in Figure 1.1, which plots the average star formation rate surface density and gas surface density within the optical radius for a selection of galaxies (Kennicutt & Evans, 2012). This relation holds for a variety of galaxies; Low Surface

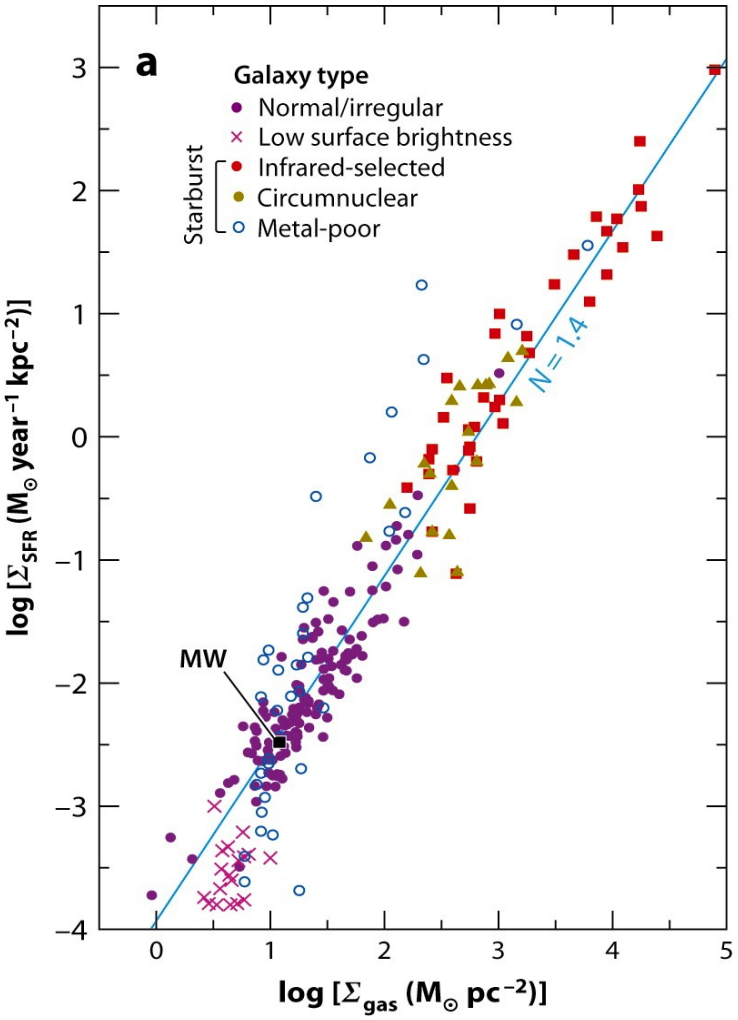

Figure 1.1 The global Kennicutt-Schmidt relation. Figure taken from Kennicutt & Evans (2012).

Brightness (LSB) galaxies, normal spirals and starburst galaxies are all plotted in Figure 1.1. There is uncertainty regarding how well galaxies actually follow this relation, and even what the power-law index should be. Since molecular hydrogen itself is not directly observable, it is traced by carbon monoxide (CO), which then requires the use of a conversion factor (X_{CO}) to discern the true H_2 content. The appropriate value for this conversion factor is often uncertain, and variations can lead to a different power-law index than expected from the usual Kennicutt-Schmidt relation (Shetty et al., 2011; Narayanan et al., 2012). As seen in Figure 1.1 certain galaxies stray more than an order of magnitude from the expected relation.

The global Kennicutt-Schmidt relation describes the average properties of galaxies with the optical radius. This relation also holds on smaller scales. The THINGS survey contains high resolution data for a sample of galaxies in the nearby universe (Walter et al., 2008). Bigiel et al. (2008) take 18 galaxies from this sample to explore the Kennicutt-Schmidt relation on local (sub-kpc) scales. The authors confirm that the Kennicutt-Schmidt relation does hold on local scales, and find a strong correlation between the molecular gas content of a galaxy and the star formation rate. Further, there is no correlation between star formation rate and atomic hydrogen content. This is seen in Figure 1.1, where there is a transition from a power-law relation at a surface density of $\sim$10 $M_\odot$ pc^{-2}, corresponding to the transition to an atomic hydrogen dominated regime.

1.1.1 Stellar Feedback

Stars return energy to their birth environments via many different mechanisms throughout their lives. These mechanisms are referred to as stellar feedback. Young stars generate UV flux. Far UV (FUV) radiation heats dust grains which will in turn heat gas. Extreme UV (EUV) radiation photo-ionizes gas surrounding the star, creating an HII region. These HII regions are a source of radiation pressure, which injects momentum into adjacent gas. Radiation pressure is a significant form of feedback for extremely luminous stars. Newly formed massive stars generate stellar winds. These winds inject energy and momentum back into the ISM (Tielens, 2005).

At the ends of their lives, massive stars will undergo explosive core-collapse (type II) supernova events (Carroll & Ostlie, 2006). Considering a cluster, for every 100 $M_\odot$ of stars formed, one star will end its life with a supernova event, depositing 10^{51} erg of energy into the surrounding ISM (Krumholz et al., 2014, and references therein).

Stellar feedback plays an important role in shaping the structure of the galaxy. It injects turbulence into the ISM, assists in making gas unavailable for star formation and shapes the clouds where stars do form. All of these processes play their own role in the equilibrium state of the ISM.

1.2 The Interstellar Medium

The ISM is home to the gas and dust that will potentially fuel star formation. The ISM has a divided phase structure, with gas preferentially existing in

Table 1.1 The Phase Structure of the ISM

Phase	T^a (K)	n_0^a (cm^{-3})	H^a pc	Mass Fraction^b (%)
Hot Ionized Medium (HIM)	$> 10^5$	0.003	3000	—
Warm Ionized Medium (WIM)	8000	0.1	900	0.13
Warm Neutral Medium (WNM)	8000	0.5	∼300	0.38
Cold Neutral Medium (CNM)	80	50	94	0.29
Molecular Clouds	10	> 200	75	0.18

^{a}Typical temperatures, densities and scale heights as listed in Tielens (2005)
^{b}Calculated based on total masses tabulated in Tielens (2005)

hot, warm or cold phases. The hot ionized medium (HIM) consists of gas with temperatures above 10^5 K. This gas is mainly heated by supernovae and lives mostly out of the plane of the galactic disc (McKee & Ostriker, 1977). Hot ionized gas is detected via UV wavelength absorption lines and X-ray emission lines. However, because of its low volume-filling fraction measurements of gas in this phase are not well constrained. For example, the mass of gas existing in this phase is uncertain (Tielens, 2005).

The warm phase consists of a warm ionized medium (WIM) and a warm neutral medium (WNM). Gas in these phases has a temperature of around 8000 K (Tielens, 2005). Warm neutral gas is detected using 21 cm line emission from HI gas. Warm ionized gas is detected using emission from the Hα recombination line and from pulsar dispersion. Lastly, the cold phase hosts the cold neutral medium (CNM) and dense molecular clouds. Cold neutral gas is detected using the 21 cm line absorption from HI gas. Molecular hydrogen

makes up the main constituent of the cloud phase. In these circumstances molecular hydrogen does not reach temperatures where emission is possible. Since it cannot be directly observed, carbon monoxide (CO) is often used as a tracer. This information is summarized in Table 1.1.

These phases reflect specific physical input from stars but also at what temperatures and densities cooling is more or less efficient. An influential idea due to Field et al. (1969) is that of thermal instability that tends to separate cooler gas into warm and cold phases. The authors show that warm and cold neutral media could exist in pressure equilibrium, producing a two-phase medium.

1.2.1 Heating and Cooling in the ISM

Heating and cooling processes provide the net energy balance in the ISM. Different mechanisms for cooling gas are dominant at different temperatures in the ISM. At low temperatures, cooling is dominated by the excitation of trace metals, such as ionized carbon (CII). At high temperatures ($T > 10^4$ K), cooling is dominated by the collisional ionization of neutral hydrogen (HI). This cooling must be balanced by a source of heating for thermal equilibrium to be maintained. Photoelectric heating is the most significant heating process for the neutral ISM though UV, included here, is also significant. Further sources of heating include cosmic rays and X-rays (Tielens, 2005). This balance between heating and cooling contributes to the two-phase structure of the ISM. In Figure 1.2 we plot the equilibrium temperature curve (solid black line), with coloured lines denoting contours of constant cooling time. When gas exists in

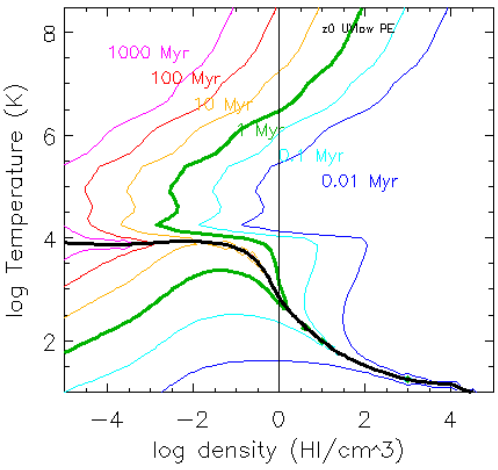

Figure 1.2 Cooling times in the interstellar medium. The solid black line denotes the equilibrium temperature for a given density. The different coloured lines denote contours of constant cooling time. Figure courtesy of James Wadsley.

the hot diffuse phase, cooling times are long. The denser gas gets, the shorter the cooling times, leading to thermal instability (gas will separate into a diffuse warm phase and a denser cold phase). Dynamics processes such as turbulence modify the outcome as seen in the results section.

1.3 The Interplay Between Stars and the ISM

Star formation is a cyclic process. Stars condense out of dense gas in the ISM. These stars unavoidably disrupt their birth environments, which in turn either promotes or discourages further star formation. If the net effect is negative feedback, we can see this process as self-regulating.

The main physical driver of this self-regulation is effective pressure. Pressure is required to balance the weight of gas in a galactic disc:

$$P_{\rm tot} = \int \rho g \, {\rm d}z \tag{1.2}$$

where $P_{\rm tot}$ is the total pressure, ρ is the gas density and g is the acceleration due to vertical gravity. Ostriker et al. (2010) argue that this process can be understood by considering that stars provide an effective pressure to the disc. Stars add to the vertical gravity in the disk and are generators of both thermal and turbulent pressure . As a result, the total pressure in the disc will correlate strongly with the amount of star formation (Ostriker et al., 2010).

This total pressure comes from both turbulent and thermal sources. The thermal pressure can be calculated as

$$P_{\rm th} = c_s^2 \rho \tag{1.3}$$

where ρ is the density of a gas particle and c_s is the sound speed,

$$c_s = \sqrt{\frac{k\gamma T}{\mu m_p}} \tag{1.4}$$

with $\mu = 1.29$, $\gamma = \frac{5}{3}$. Sources of thermal pressure include stellar feedback, UV radiation and photoelectric heating. The turbulent pressure can be calculated as

$$P_{\rm turb} = v_z^2 \rho \tag{1.5}$$

where v_z is the vertical velocity component of a gas particle. Sources of turbulent pressure include stellar feedback and galactic shear. It is these factors which will balance the weight of the ISM and regulate star formation to its equilibrium state (Ostriker et al., 2010).

The role of self-regulation can be seen empirically in the Kennicutt-Schmidt relation (see Figure 1.1). However, while all types of galaxies appear to lie close to the power-law relation, it is clear that different types of galaxies occupy different regimes of the plot. This fact is due to the mechanisms by which star formation self-regulates. Above 100 $M_\odot$ pc^{-2}, in the upper right-hand portion of the plot live starburst galaxies (red, gold and blue points). In starburst galaxies the ISM is composed almost completely of molecular gas and as a result they have very high star formation rates and efficiencies (Solomon & Vanden Bout, 2005). In these environments turbulence is very important to star formation (Shetty & Ostriker, 2012; Faucher-Giguère et al., 2013). Normal galaxies live between $\sim$ 10 and 100 $M_\odot$ pc^{-2} (filled purple circles). Here FUV heating is instead the dominant mechanism of regulation (Ostriker et al., 2010). Low surface brightness (LSB) galaxies are found at gas surface densities below $\sim$ 10 $M_\odot$ pc^{-2} (purple crosses). In this case, it is perhaps the inability of gas to easily form a cold phase via thermal instabilities which limits the rate of star formation (Schaye, 2004).

What we can take away from this is that the formation of a cold medium is the rate limiting step for star formation. This cold phase is needed to host the formation of molecular hydrogen gas. In starburst galaxies this is not so crucial, as the ISM is already mainly composed of H_2 and so star formation is extremely efficient. In LSB galaxies however, the ISM is dominated by atomic hydrogen. In Figure 1.1 it is these galaxies which clearly fall away from the expected relation, implying interesting physics. This is a similar composition to what is seen in the outer edges of normal galactic discs and provides us with

a laboratory to explore how large a role the availability of a cold phase plays in setting the star formation rate.

The Toomre Q parameter is a measure used to describe the degree to which gas in a thin disc is gravitationally unstable.

$$Q = \frac{\kappa \sigma_g}{\pi G \Sigma_g} \tag{1.6}$$

where κ is the epicycle frequency, σ_g is the gas velocity dispersion and Σ_g is the gas surface density. Collections of gas with $Q < 1$ are considered gravitationally unstable. Although this can be used to judge for instability, it is not a reliable measure to correlate available gas with actual star formation events (Leroy et al., 2008).

Elmegreen & Parravano (1994) first proposed that it is not the Q parameter that dictates what gas will form stars, but rather the presence of a two phase medium in pressure equilibrium. Gerritsen & Icke (1997) employ N-body simulations to show that stars can form only from gas existing in the cold dense/phase of the ISM. The importance of this cold phase separation for star formation is further reinforced by Hunter et al. (1998) and Elmegreen (2002).

Through the use of analytical models, Schaye (2004) applies this idea to the outer discs of galaxies. There is a clear radius in galaxies where star formation is sharply truncated. This truncation is well supported by observational evidence. In these regions there is a decrease in the thermal velocity dispersion, $\sigma_{\rm th}$. This drastic drop is associated with the transition from a warm to a cold gas phase, and is responsible for triggering gravitational instability. This corresponds to a critical surface density, $\Sigma_{\rm crit}$, below which it is not possible

to support large-scale star formation. The critical surface density should fall between 3-10 $M_\odot$ pc^{-2}, corresponding to a pressure, P/k, between 100-1000 cm^{-3}. This phenomenon is possible on a large range of scales, and can proceed even in the presence of turbulent support (Schaye, 2004).

1.4 Numerical Studies of the ISM

Star formation is a process involving many scales and is heavily influenced by the galactic environment. At the core of questions involving the ISM and star formation lie GMCs. GMCs exist within the cold/dense phase of the ISM and hold the fuel for star formation. The most direct way to study this cold phase is through the use of numerical simulations. There are two tactics when considering how to approach this problem. One can use high resolution simulations of small regions, focusing on the formation of small numbers of GMCs in a local context (see for example Heitsch et al. (2008), Ntormousi et al. (2011)). Moving up one scale, one can instead sacrifice resolution but include the whole galactic disc environment. When considering which approach to use, one must keep in mind that the three main drivers of structure in galactic discs are thought to be galactic shear, the two-phase instability, and star formation/stellar feedback. It is the interplay of these drivers which regulates GMC formation and, consequently, star formation. In order to include all of this physics, the most desirable approach, and the approach we use in this thesis, is to employ full galactic disc simulations.

This is a deceptively difficult problem to attack. The formation of a cold phase in simulations is extremely resolution sensitive. As well the physics in-

volved is non-linear; the interplay between star formation, feedback, and the structure of the ISM is in no way straight-forward. Further, turbulence is generated at the largest scales of the galaxy and then cascades down to smaller scales. Simulations have difficulty with this cascade, and holding turbulent power on GMC scales in the ISM.

This problem has been heavily studied in recent years. Tasker & Tan (2009) and Tasker (2011) employ simulations of a Milky Way type galaxy, both with and without star formation, respectively. In cases with no star formation, gas is allowed to collect without any form of regulation. This unchecked buildup can lead to cases of runaway collapse. Dobbs et al. (2011) study GMC formation in galactic discs with strong spiral structure. This structure is meant to model the strong spiral patterns associated with a nearby perturber, similar to the case of M51 and its companion. These simulations include stellar feedback. The authors are able to produce a fraction of cold gas consistent with observations. Bonnell et al. (2013) debut a new approach by perfuming a low resolution simulation of a full galactic disc and then harvesting interesting regions for re-simulation at higher resolution.

1.4.1 The Impacts of Numerical Choices

Studies of the ISM employing simulations often require the use of recipes for unresolvable physics. Hopkins et al. (2011) explore the impact of changing the choice of star formation parameters on the ISM. The authors find that the star formation rate is largely insensitive to parameters associated with the star formation law. However, the processes related to stellar feedback are

extremely important. Further, Hopkins et al. (2012) find that the type of stellar feedback employed has a large impact on the outcome of the simulation. The authors compare the effects of energy and momentum injection from types I and II supernovae, stellar winds, radiation pressure and HII photo-ionization. Agertz et al. (2013) and Agertz & Kravtsov (2014) also explore this parameter dependence with similar findings.

1.5 Overview

The relationship between star formation and the evolution of galaxies involves a great deal of interconnected physics. In order to better understand these connections it is desirable to use a suite of many simulations, where each process can be explored in a controlled set-up. For these reasons, we have chosen to follow a different approach from those discussed above. We have modelled a relatively quiet isolated galaxy with no old stellar population and no perturbers. The choice of an isolated galaxy excludes the effects of complicated environmental factors such as mergers, cosmic evolution and a lack of axi-symmetry. While our galaxy is quiet, we have included both star formation and extremely efficient feedback, all done at high resolution.

The remainder of the thesis will proceed as follows. In Chapter 2 we outline the simulation code GASOLINE and what we have added to it for this work. We also introduce our method for the generation of initial conditions for our galactic discs. Chapter 3 lists the suite of simulations employed and discusses our findings from these simulations. Finally, in Chapter 4 we give concluding remarks and discuss thoughts for future work.

Bibliography

Agertz, O. & Kravtsov, A. V. 2014, ArXiv e-prints

Agertz, O., Kravtsov, A. V., Leitner, S. N., & Gnedin, N. Y. 2013, ApJ, 770, 25

Bigiel, F., Leroy, A., Walter, F., Brinks, E., de Blok, W. J. G., Madore, B., & Thornley, M. D. 2008, AJ, 136, 2846

Bonnell, I. A., Dobbs, C. L., & Smith, R. J. 2013, MNRAS, 430, 1790

Carroll, B. W. & Ostlie, D. A. 2006, An introduction to modern astrophysics and cosmology

Dobbs, C. L., Burkert, A., & Pringle, J. E. 2011, MNRAS, 417, 1318

Elmegreen, B. G. 2002, ApJ, 577, 206

Elmegreen, B. G. & Parravano, A. 1994, ApJ, 435, L121

Faucher-Giguère, C.-A., Quataert, E., & Hopkins, P. F. 2013, MNRAS, 433, 1970

Field, G. B., Goldsmith, D. W., & Habing, H. J. 1969, ApJ, 155, L149

Gerritsen, J. P. E. & Icke, V. 1997, A&A, 325, 972

Heitsch, F., Hartmann, L. W., Slyz, A. D., Devriendt, J. E. G., & Burkert, A. 2008, ApJ, 674, 316

Hopkins, P. F., Quataert, E., & Murray, N. 2011, MNRAS, 417, 950

—. 2012, MNRAS, 421, 3488

Hunter, D. A., Elmegreen, B. G., & Baker, A. L. 1998, ApJ, 493, 595

Kennicutt, R. C. & Evans, N. J. 2012, ARA&A, 50, 531

Kennicutt, Jr., R. C. 1998, ApJ, 498, 541

Krumholz, M. R., Bate, M. R., Arce, H. G., Dale, J. E., Gutermuth, R., Klein, R. I., Li, Z.-Y., Nakamura, F., & Zhang, Q. 2014, ArXiv e-prints

Krumholz, M. R. & Tan, J. C. 2007, ApJ, 654, 304

Lada, C. J., Lombardi, M., & Alves, J. F. 2010, ApJ, 724, 687

Leroy, A. K., Walter, F., Brinks, E., Bigiel, F., de Blok, W. J. G., Madore, B., & Thornley, M. D. 2008, AJ, 136, 2782

Leroy, A. K., Walter, F., Sandstrom, K., Schruba, A., Munoz-Mateos, J.-C., Bigiel, F., Bolatto, A., Brinks, E., de Blok, W. J. G., Meidt, S., Rix, H.-W., Rosolowsky, E., Schinnerer, E., Schuster, K.-F., & Usero, A. 2013, AJ, 146, 19

McKee, C. F. & Ostriker, E. C. 2007, ARA&A, 45, 565

McKee, C. F. & Ostriker, J. P. 1977, ApJ, 218, 148

Narayanan, D., Krumholz, M. R., Ostriker, E. C., & Hernquist, L. 2012, MNRAS, 421, 3127

Ntormousi, E., Burkert, A., Fierlinger, K., & Heitsch, F. 2011, ApJ, 731, 13

Ostriker, E. C., McKee, C. F., & Leroy, A. K. 2010, ApJ, 721, 975

Schaye, J. 2004, ApJ, 609, 667

Schmidt, M. 1959, ApJ, 129, 243

Shetty, R., Glover, S. C., Dullemond, C. P., & Klessen, R. S. 2011, MNRAS, 412, 1686

Shetty, R. & Ostriker, E. C. 2012, ApJ, 754, 2

Solomon, P. M. & Vanden Bout, P. A. 2005, ARA&A, 43, 677

Tasker, E. J. 2011, ApJ, 730, 11

Tasker, E. J. & Tan, J. C. 2009, ApJ, 700, 358

Tielens, A. G. G. M. 2005, The Physics and Chemistry of the Interstellar Medium

Walter, F., Brinks, E., de Blok, W. J. G., Bigiel, F., Kennicutt, Jr., R. C., Thornley, M. D., & Leroy, A. 2008, AJ, 136, 2563

Chapter 2

Methods

2.1 Smoothed Particle Hydrodynamics

Smoothed Particle Hydrodynamics (SPH) is a Lagrangian method to computationally model fluid flows (Lucy, 1977; Gingold & Monaghan, 1977). In SPH, continuous fluids are represented by collections of discrete particles. Specific physical quantities of these fluids can then be obtained by summing over all nearby particles. This calculation will be done for particles within a characteristic smoothing length, h. The summation requires the use of weighting for each particle. In order to create a smoothed fluid distribution, these weights are generated by a chosen smoothing kernel, W. The smoothing kernel must satisfy a set of conditions. These conditions are:

$$\int W(|\mathbf{r}-\mathbf{r}'|,h)d\mathbf{r}=1 \tag{2.1}$$

and

$$\lim_{h\to 0} W(|\mathbf{r}-\mathbf{r}'|,h)=\delta_D(\mathbf{r}-\mathbf{r}') \tag{2.2}$$

where δ_D is the Dirac delta function (Monaghan, 1992). These conditions require that the kernel be normalized to a value of 1. The kernel can then be used to calculate a chosen property of the fluid, $A(\mathbf{r})$, by

$$A(\mathbf{r}) \sim \sum_{i=1}^{N} m_i \frac{A_i}{\rho_i} W(|\mathbf{r} - \mathbf{r}'_i|, h) d\mathbf{r}' \tag{2.3}$$

where m_i is the mass of an individual particle, ρ_i is the density of an individual particle and N the number of neighbours smoothed over. For this work the typical number of neighbours required is 64.

For the simulations discussed in this thesis, we employ a Wendland C^2 kernel function (Dehnen & Aly, 2012). The functional form is

$$W(\mathbf{x}, h) = \frac{w(\mathbf{x})}{h^3} = \frac{21}{6\pi h^3}(1-q)^4(1+4q) \tag{2.4}$$

where $q = x/h$. This is different from the usual spline smoothing kernel

$$W(\mathbf{x}, h) = \frac{1}{\pi h^3} \begin{cases} 1 - \frac{3}{2}q^2 + \frac{3}{4}q^3 & : \ 0 \leq q < 1, \\ \frac{1}{4}(2-q)^3 & : \ 1 \leq q < 2, \\ 0 & : \ otherwise \end{cases} \tag{2.5}$$

(Monaghan & Lattanzio, 1985). For comparison, the two kernels are plotted in Figure 2.1. Choosing a Wendland kernel does not allow pairing of particles. It also allows the possibility of smoothing over a larger number of neighbours if desired (e.g. 200 neighbours rather than the typical 32 or 64). **We choose the Wendland kernel because our feedback algorithm, described in the next section, was developed to work with it.**

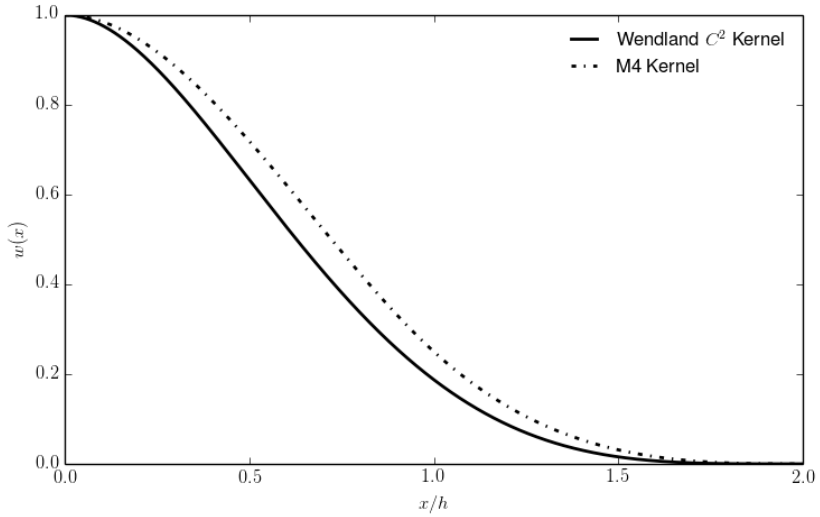

Figure 2.1 The chosen Wendland C^2 smoothing kernel (Dehnen & Aly, 2012), plotted as a function of x/h. For comparison, the dashed-dotted line shows the usual M4 spline kernel (Monaghan & Lattanzio, 1985)

2.2 GASOLINE

We employ the SPH simulation code GASOLINE (Wadsley et al., 2004). GASOLINE is built on the gravity solver PKDGRAV (Stadel, 2001). It includes radiative metal line cooling (Shen et al., 2010), as well as subgrid recipes for star formation and supernovae (SNe) feedback (Stinson et al., 2006; Keller et al., 2014). The specific treatments we use for star formation and supernova feedback are outlined in the sections that follow. For this thesis, we have added treatment for photoelectric heating to GASOLINE.

2.2.1 Star Formation

Star particles are created by taking a fraction of the mass of an eligible gas particle. In order to be considered eligible to form stars, a gas particle must first pass three criteria:

1. it must have a density $n > n_{\rm th}$
2. it must have a temperature, $T < T_{\rm max}$
3. it must be part of a converging flow ($\nabla \cdot v < 0$)

where $n_{\rm th}$ and $T_{\rm max}$ are the chosen density and temperature thresholds, respectively. Eligible gas particles are then stochastically chosen to form stars, based on the relation

$$\frac{{\rm d}M_*}{{\rm d}t} = c_* \frac{M_{\rm gas}}{t_{\rm dyn}} \tag{2.6}$$

where $M_{\rm gas}$ is the mass of the gas involved, M_* is the mass of the stars created, $t_{\rm dyn} = 1/\sqrt{4\pi G\rho}$ is the dynamical time and c_* is a constant efficiency factor (Stinson et al., 2006). In Section 2.2.1 we explore the consequences for specific choices of $n_{\rm th}$ and c_*.

2.2.2 Feedback

We employ supernova feedback similar to the methods used in Agertz et al. (2013), as described in Keller et al. (2014). Supernovae deposit 10^{51} erg of energy into the surrounding ISM. Based on the stellar initial mass function of Chabrier (2003), approximately one in 100 stars will undergo a supernova event, resulting in an average supernova energy of 10^{49} erg/$\rm M_\odot$. In this method,

feedback energy, $E_{\rm FB}$, has radiative cooling disabled. The relevant energy equations are then

$$\frac{{\rm d}E_{\rm C}}{{\rm d}t} = \frac{E_{\rm NC}}{\tau} + P{\rm d}V - \Lambda \tag{2.7a}$$

$$\frac{{\rm d}E_{\rm NC}}{{\rm d}t} = -\frac{E_{\rm NC}}{\tau} + P{\rm d}V - E_{\rm FB} \tag{2.7b}$$

where $E_{\rm C}$ is the cooling energy, $E_{\rm NC}$ is the non-cooling energy and Λ is the cooling rate. Feedback energy is then steadily converted back into the regular, cooling form. This occurs over a chosen conversion timescale, τ. For the purpose of this work, we adopt a conversion time of $\tau = 5$ Myr. This energy deposition due to supernovae will begin immediately after a star forms. This is done to mimic early stellar feedback processes, such as stellar winds.

2.2.3 Photoelectric Heating

The dominant source of heating due to photoelectric absorption by dust grains comes from ultraviolet (UV) radiation from stars (Watson, 1972). The heating rate due to photoelectric heating is set by

$$n\Gamma_{\rm PE} = 10^{-24}\epsilon n G_0 \text{ erg cm}^{-3} \text{ s}^{-1} \tag{2.8}$$

where *epsilon* represents a heating efficiency, G_0 is the intensity of the radiation field in units of the average interstellar radiation field and n is the number density of the gas. Here we assume that $\epsilon G_0 \sim 0.05$ (Tielens, 2005). To model

this photoelectric heating throughout the disc we employ a Far Ultra-Violet (FUV) heating term:

$$n\Gamma_{\rm FUV} = n\Gamma_{\rm PE} \times \begin{cases} e^{-(4-R_0)/4} & : \quad R < 4 \text{ kpc} \\ e^{-(R-R_0)/4} & : \quad R \geq 4 \text{ kpc} \end{cases} \tag{2.9}$$

with $R_0 = 8.5$ kpc. This functional form is chosen to approximate the model of ISM structure predicted by Wolfire et al. (2003). With this set functional form, the FUV heating is decoupled from actual star formation events.; gas will be heated even where there are no stars present. While this distribution does not trace actual star formation in our simulations, it does trace the expected distribution of gas in the Milky Way (Wolfire et al., 2003). Star formation should trace the distribution of density and so we expect our FUV heating to approximate the distribution of stars in our galaxy. We also approximate the depletion of elements onto dust grains via freeze-out. This is done by multiplying the total metal abundance by a constant depletion factor of 0.4 (Tielens, 2005).

2.3 The Initial Conditions

Here we describe the process used to generate our initial conditions. We model an isolated, quiescent disc galaxy. This is similar to the approach followed by Dobbs et al. (2011).

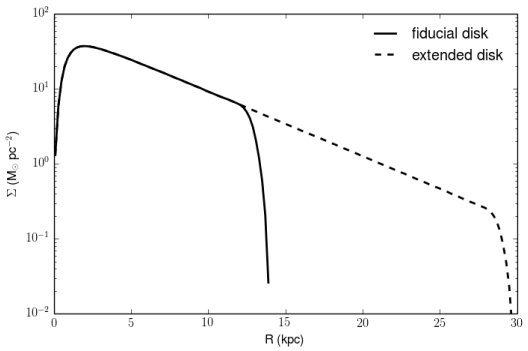

Figure 2.2 A surface density profile for two of the isolated disc ICs. The black solid line depicts a typical disc, truncated at a radius of 14 kpc. The black dashed line depicts an extended disc, truncated at a radius of 30 kpc. Both discs normalized to a surface density of 14 $M_\odot$ pc^{-2} at R_0.

2.3.1 Density Profile

We model an isolated disc galaxy with a density profile decreasing exponentially with radius as follows,

$$\Sigma_g(r) = \Sigma_0 \left(\frac{r^2}{r^2 + 1} \right) e^{(-(r-8)/5)} \tag{2.10}$$

where Σ_0 is the chosen density at the solar radius. We have chosen two values to explore, $\Sigma_0 = 7$ and 14 $M_\odot$ pc^{-2}. These choices of surface density are motivated by estimates of the ISM surface density at the solar radius found in Binney & Tremaine (2008). When varying the normalization density, Σ_0, the particle mass is held constant to ensure the physics is unchanged. As a result, discs with different Σ_0 have different total mass. Our chosen values of 7 and 14 $M_\odot$ pc^{-2} result in discs with total masses of 3.75×10^9 and 7.51×10^9 $M_\odot$, respectively. For comparison, the gas mass of the Milky Way is approximately 4.5×10^9 $M_\odot$ (Tielens, 2005).

The centers of galaxies are extrememly dense regions, impacted heavily by the presence of active galactic nuclei (AGN). For the purpose of this study

we are not interested in the physics of AGN. So to conserve resolution, we exclude the center of the disc, within the inner 1 kpc. At the outer edge, we also truncate the disc:

$$\Sigma_g(r) = \begin{cases} \Sigma_g & : \quad r < R_1, \\ \Sigma_g \times \left(\frac{1-2(r-R_1)}{R_2-R_1}\right)^2 & : \quad R_1 \leq r < \frac{1}{2}(R_1+R_2), \\ \Sigma_g \times 2\left(\frac{R_2-r}{R_2-R_1}\right)^2 & : \quad r > \frac{1}{2}(R_1+R_2) \\ 0 & : \quad r > R_2 \end{cases} \tag{2.11}$$

where R_1 and R_2 denote the radii which span the region where the disc will be truncated. For most of our discs, R_1 and R_2 are set to 12 and 14 kpc, respectively. The initial density profile for a disc normalized to $\Sigma_0 = 14$ $M_\odot$ pc^{-2} can be seen in Figure 2.2. To study structure in the outer disc region, we also construct an extended disc, with R_1 and R_2 set to 28 and 30 kpc, respectively.

The temperature in the disc is initialized at 300 K. The choice of initial particle temperature does not have a large impact on the properties of the disc. In Figure 2.3 the results of changing the initial temperature from 300 to 5000 K are shown. This change has very little impact on either the global star formation rate and the density distribution.

2.3.2 Turbulence

The simulations are initialized with a turbulent velocity field in the x, y, and z directions. This field is random with a Kolmogorov ($k^{-5/3}$) spectrum. The velocity perturbations were smoothly tapered to zero away from the mid-plane. The initial root mean square velocity is ~ 10 km s^{-1}. This is a typical

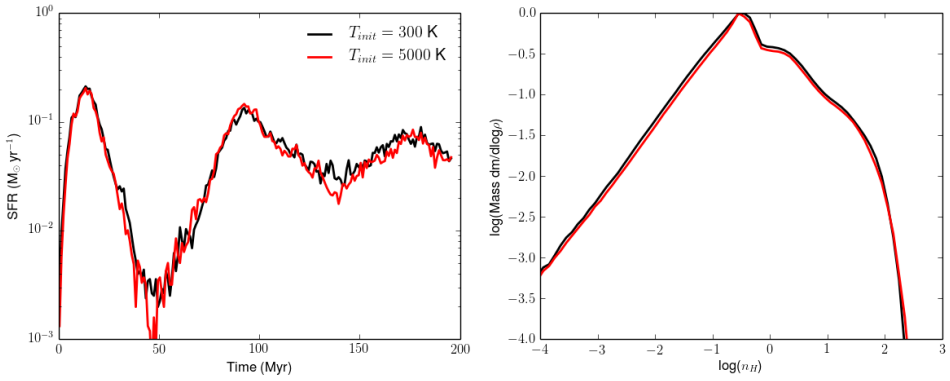

Figure 2.3 The effect of changing the choice of $T_{\rm init}$ for the disc. Left panel: Star formation rate. Right panel: Distribution of densities after 200 Myr of evolution. Neither of these quantities is largely impacted by changing the initial temperature from 300 to 5000 K.

value observed for neutral atomic gas (Tamburro et al., 2009). At late times, the simulations are not sensitive to this initial choice. We ensure that all simulations included in this analysis have been evolved long enough to establish self-consistent galactic structure. We estimate that this point in time should be $\sim$ 200-250 Myr, since the time for the galaxy to complete one rotation at the solar radius is 240 Myr.

2.3.3 Evolution

The disc is evolved in a static dark matter halo potential. A log halo potential is used:

$$\Phi_{\rm L} = \frac{1}{2}v_0^2 \ln\left(R_c^2 + R^2 + \frac{z^2}{q_\Phi^2}\right) \tag{2.12}$$

where the circular speed at a chosen radius would be:

$$v_c = \frac{v_0 R}{\sqrt{R_c^2 + R^2}} \tag{2.13}$$

(Binney & Tremaine, 2008). For our galaxy, $q_\Phi = 1$, $R_c = 1$ kpc, and $v_0 = 220$ km s^{-1}. We choose v_c to match the rotation velocity at the solar radius in the Milky Way (Binney & Tremaine, 2008).

2.4 Consequences of the Photoelectric Heating Term

As described in section 2.2.3, we implement a FUV heating term to model the two-phase structure of the ISM seen in Wolfire et al. (2003). Since the term varies exponentially with radius, it has a different effect on the structure of the ISM at different locations in the disc. Figure 2.4(top panel) shows a sample phase diagram for one of our simulations, coloured by mass. Redder colours mark regions in $T - n$ space where there is a large amount of mass, and vice versa for bluer colours. There are visible tracks through the $T - n$ space where there is a build-up of mass. Figure 2.4(bottom panel) shows this phase diagram again, however, it is now coloured by the radial xy-position of the gas particles (a subset of every 100 particles is sampled to make the plot easier to interpret). Comparing this to the mass-weighted phase diagram, we can see that the tracks of high mass build-up correspond to particles living at different radii in the disc. This is attributed to the radially varying FUV heating term.

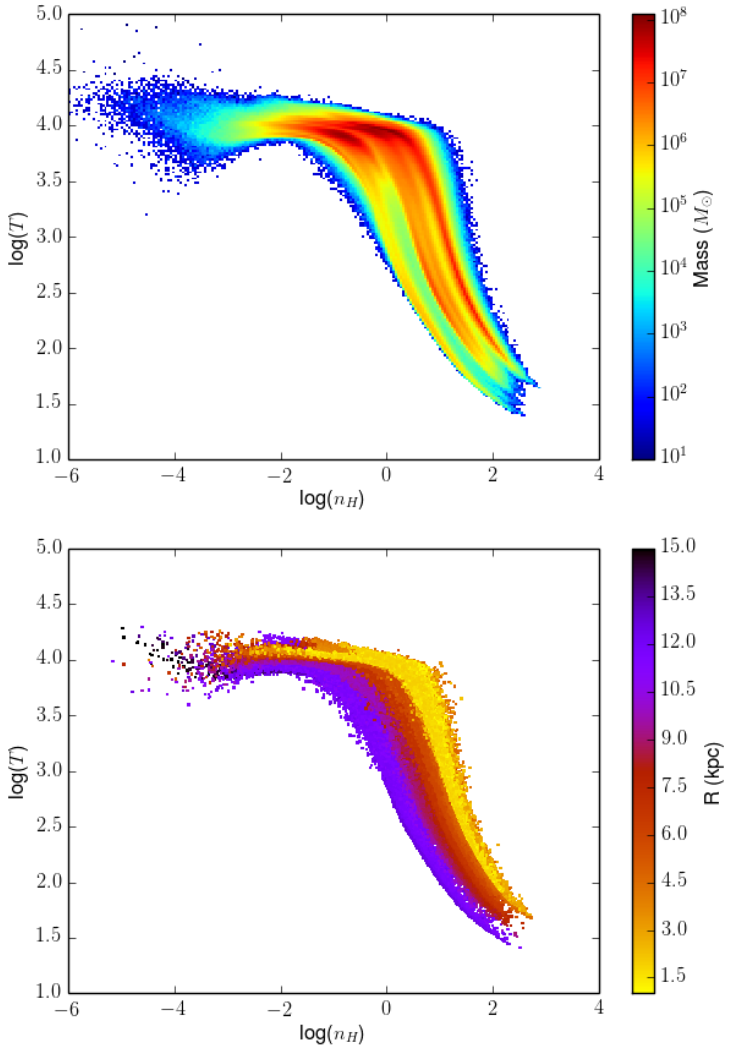

Figure 2.4 The effect of the radially varying FUV heating term on the phases of the ISM. Top panel: A phase diagram for simulation s14.n100.c1.5 (see Table 3.1 for naming convention). Large portions of the mass in the ISM congregate onto tracks. Bottom panel: Same as top but colour-coded by radius and here only every 100 particles are sampled The tracks in the top panel correspond to gas at different radii in the disc.

Bibliography

Agertz, O., Kravtsov, A. V., Leitner, S. N., & Gnedin, N. Y. 2013, ApJ, 770, 25

Binney, J. & Tremaine, S. 2008, Galactic Dynamics: Second Edition (Princeton University Press)

Chabrier, G. 2003, PASP, 115, 763

Dehnen, W. & Aly, H. 2012, MNRAS, 425, 1068

Dobbs, C. L., Burkert, A., & Pringle, J. E. 2011, MNRAS, 417, 1318

Gingold, R. A. & Monaghan, J. J. 1977, MNRAS, 181, 375

Keller, B. W., Wadsley, J., Benincasa, S. M., & Couchman, H. M. P. 2014, MNRAS, 442, 3013

Lucy, L. B. 1977, AJ, 82, 1013

Monaghan, J. J. 1992, ARA&A, 30, 543

Monaghan, J. J. & Lattanzio, J. C. 1985, A&A, 149, 135

Shen, S., Wadsley, J., & Stinson, G. 2010, MNRAS, 407, 1581

Stadel, J. G. 2001, PhD thesis, UNIVERSITY OF WASHINGTON

Stinson, G., Seth, A., Katz, N., Wadsley, J., Governato, F., & Quinn, T. 2006, MNRAS, 373, 1074

Tamburro, D., Rix, H.-W., Leroy, A. K., Mac Low, M.-M., Walter, F., Kennicutt, R. C., Brinks, E., & de Blok, W. J. G. 2009, AJ, 137, 4424

Tielens, A. G. G. M. 2005, The Physics and Chemistry of the Interstellar Medium

Wadsley, J. W., Stadel, J., & Quinn, T. 2004, New A, 9, 137

Watson, W. D. 1972, ApJ, 176, 103

Wolfire, M. G., McKee, C. F., Hollenbach, D., & Tielens, A. G. G. M. 2003, ApJ, 587, 278

Chapter 3

Simulation Results & Discussion

3.1 Simulations

Using methods described in Chapter 2, we employ a suite of high resolution simulations to study the structure of the interstellar medium in isolated galaxies. Our simulations cover a wide parameter space; the full suite is listed in Table 3.1. Simulations are named following the convention s{Σ_0}. n{$n_{\rm th}$}. c{c_*}. {comments}. For instance, a simulation with $\Sigma_0 = 7$ M$_\odot$ pc^{-2}, $n_{\rm th} = 100$ cm^{-3}, and $c_* = 6\%$ would be named s7.n100.c6. In the comments space, *low*/*high* refer to resolution, x refers to extended discs and $FUVR_0$ refers to simulations with a uniform FUV heating term. For all simulations with a uniform FUV heating, the rate is clamped to its value at the solar radius. A comment of*lowFB* refers to simulations with $\epsilon_{\rm FB} = 10\%$. We define $\epsilon_{\rm FB} = 10\%$ as the percentage of the 10^{51} ergs available from supernovae feedback that will be released into the gas; 10% then corresponds to an energy of 10^{50} ergs.

In this chapter we describe the analysis performed on this suite. As discussed in Section 2, parameters must be chosen for the star formation and

Table 3.1 List of Simulations

name	m_g ($M_\odot$)	Σ_0 ($M_\odot$ pc^{-2})	n_{th} (cm^{-3})	c_* (%)	$\epsilon_{\rm FB}$ (%)	t_f (Myr)
s7.n10.c0.35	441.94	7	10	0.35	100	250
s7.n10.c1.5	441.94	7	10	1.5	100	250
s7.n10.c6	441.94	7	10	1.5	100	240
s7.n100.c6	441.94	7	100	6	100	300
s7.n100.c6.lowFB	441.94	7	100	6	10	300
s7.n100.c6.highT	441.94	7	100	6	100	245
s7.n100.c1.5	441.94	7	100	1.5	100	300
s7.n100.c0.35	441.94	7	100	0.35	100	300
s7.n1000.c6	441.94	7	10^3	6	100	475
s7.n1000.c6.lowFB	441.94	7	10^3	6	100	265
s7.n1000.c1.5	441.94	7	10^3	1.5	100	200
s7.n100.c6.low	3535.53	7	100	6	100	300
s7.n100.c6.high	55.24	7	100	6	100	300
s7.n1000.c6.high	55.24	7	10^3	6	100	250
s14.n10.c0.35	441.94	14	10	0.35	100	190
s14.n10.c6	441.94	14	10	6	100	235
s14.n100.c0.35	441.94	14	100	0.35	100	300
s14.n100.c1.5	441.94	14	100	1.5	100	300
s14.n100.c6	441.94	14	100	6	100	300
s14.n1000.c1.5	441.94	14	10^3	1.5	100	400
s14.n1000.c6	441.94	14	10^3	6	100	220
s14.n10^4.c5	441.94	14	10^4	5	100	255
s14.n10^4.c5.lowFB	441.94	14	10^4	5	10	255
s14.n10^4.c5.lowFB.x	441.94	14	10^4	5	10	400
s14.n10^4.c5.lowFB.x.FUVR$_0$	441.94	14	10^4	5	10	400

feedback recipes. We begin by exploring the consequences of different choices for these parameters. As well, we present a resolution study to confirm convergence at our chosen fiducial resolution ($m_p = 441.94$ M$_\odot$). With this in mind we then use a sub-sample of the suite to study the causes of the truncation of star formation in the outer edges of galactic discs.

For the remainder of this chapter we use the following definitions. With regards to temperature, we subdivide the ISM into four categories; cold ($T <$ 150 K), intermediate ($150 < T <$ 5000 K), warm ($5000 < T < 10^5$ K), and hot ($T > 10^5$ K). We choose to define young stars as those with an age of less than 100 Myr. This allows us to average over a large enough time period that we can minimize the effects of any transient structures.

3.1.1 Initial Analysis

We begin by showing a basic analysis for each of the simulations in the suite. Figures 3.1 and 3.2 show the global star formation rate for each galaxy with the simulation name labelled in the upper right hand corner. Many of the galaxies shown here have low star formation rates; for comparison the star formation rate of the Milky Way is approximately 2 M$_\odot$ yr^{-1} (Kennicutt & Evans, 2012, and references therein). This is especially true for the low surface density discs, which have average star formation rates of approximately 0.1 M$_\odot$ yr^{-1}. This may be due to the fact that the discs do not contain the central regions, where the surface density is high and there is expected to be a large amount of star formation. If the regulation of star formation is non-linear, excluding such high density regions can have a large suppressing effect on the

star formation rate without significantly lowering $\Sigma_{\rm SFR}$ and $\Sigma_{\rm g}$. Further, our discs are meant to model un-perturbed galaxies and so we would expect the star formation rate to be lower. For example, as shown in Figure 1.1, there are galaxies that deviate an order of magnitude below the mean value in the Kennicutt-Schmidt relation.

Figures 3.3 and 3.4 show phase diagrams for each galaxy. First, there is a notable difference between the low and high surface density discs in this respect. Gas in the low surface density discs lives mostly along the equilibrium temperature curve. Only in the high surface density discs do we see any spread (from turbulence) and any feedback heated gas with $T > 10^4$ K.

Figures 3.5 and 3.6 show the scale heights and gas fractions for three temperature ranges in our ISM. The data is plotted in 100 Myr intervals. This analysis is only shown for the high surface density discs. In the low surface density discs, gas fraction and scale heights for cold and intermediate gas are too small to gain any insight from these cases. The different simulations have vastly varying scale heights and gas fractions; some general trends are noticeable however. It appears that increasing the density threshold increases the fraction of cold gas. Cases with lower feedback efficiency also appear to have higher cold gas fractions.

Figures 3.7 and 3.8 show face-on density projections for each galaxy. These images show a prominent ring feature in the discs. These features are not transient, although they are not present in all cases. These rings may be due to a resonance created by the profiles chosen for the initial surface density and the FUV heating distribution. Another possibility is that these rings are

due to early bursts of star formation. The initial density profiles of the discs means that the centres are densest and so become available for star formation first. Stars will form very quickly towards the centre and then all produce supernovae at the same time. This scenario is supported by the fact that in some cases, the ring structures appear to emanate out from the centres of the discs over time. These ring structures are less prominent in cases with low feedback efficiency. This may indicate that our fiducial level of feedback is too high and our low efficiency cases are more realistic.

We finish this initial analysis by plotting a sample of our galaxies on the global Kennicutt-Schmidt relation. Here, we define the optical radius of our simulated galaxies as the half mass radius of the stellar component. Figure 3.9 shows the global Kennicutt-Schmidt law for a selection of the galaxies in our sample. We plot the star formation rate surface density ($\Sigma_{\rm SFR}$) for young stars as a function of the total gas surface density ($\Sigma_{\rm gas}$) within our estimated optical radius. One can see that increasing $n_{\rm th}$ increases $\Sigma_{\rm SFR}$, moving a galaxy vertically upwards while remaining at the same $\Sigma_{\rm gas}$. The only galaxies in our sample lying close to the expected power-law index of $N = 1.4$ are the galaxies with lowered feedback efficiency (denoted by squares on the plot).

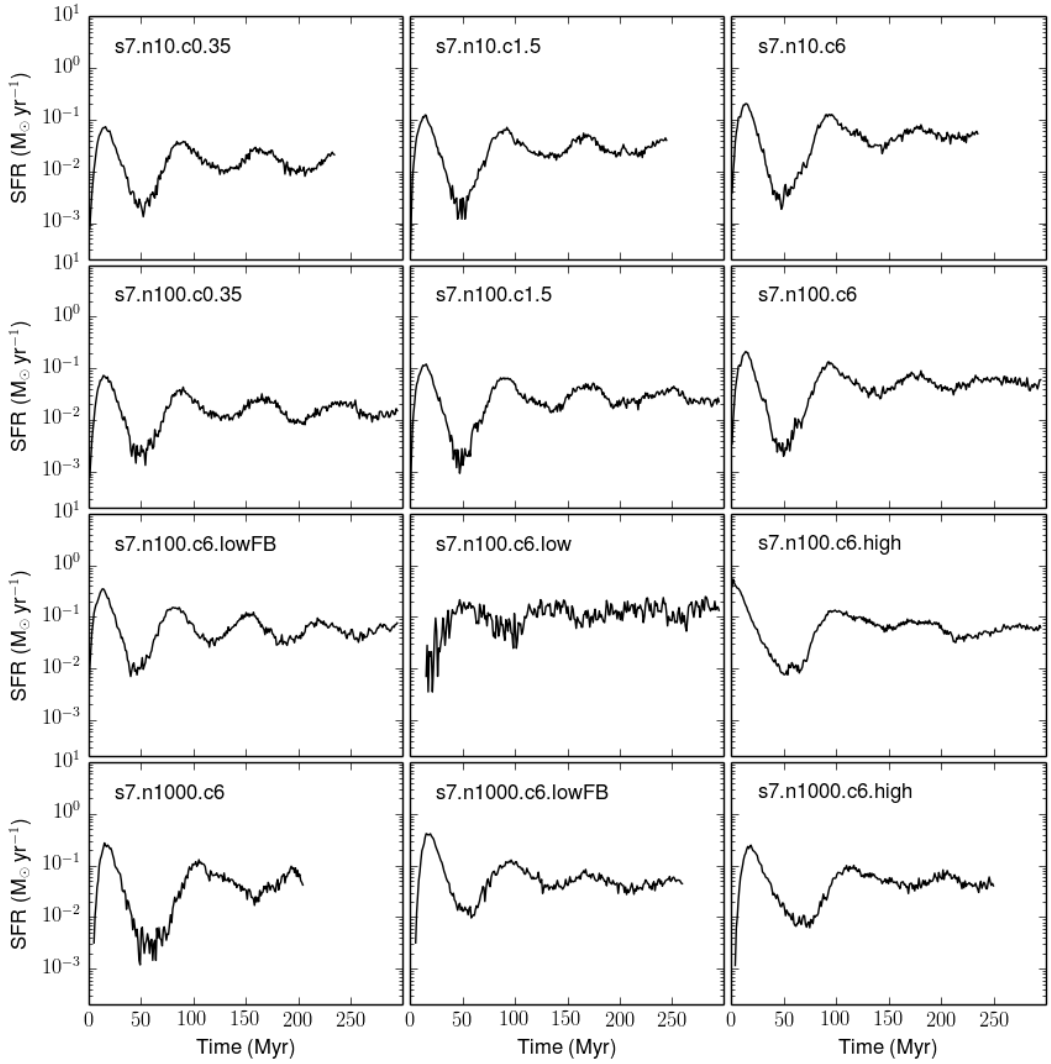

Figure 3.1 The star formation rates for our low surface density discs ($\Sigma_0 = 7$ $M_\odot$ pc^{-2}).

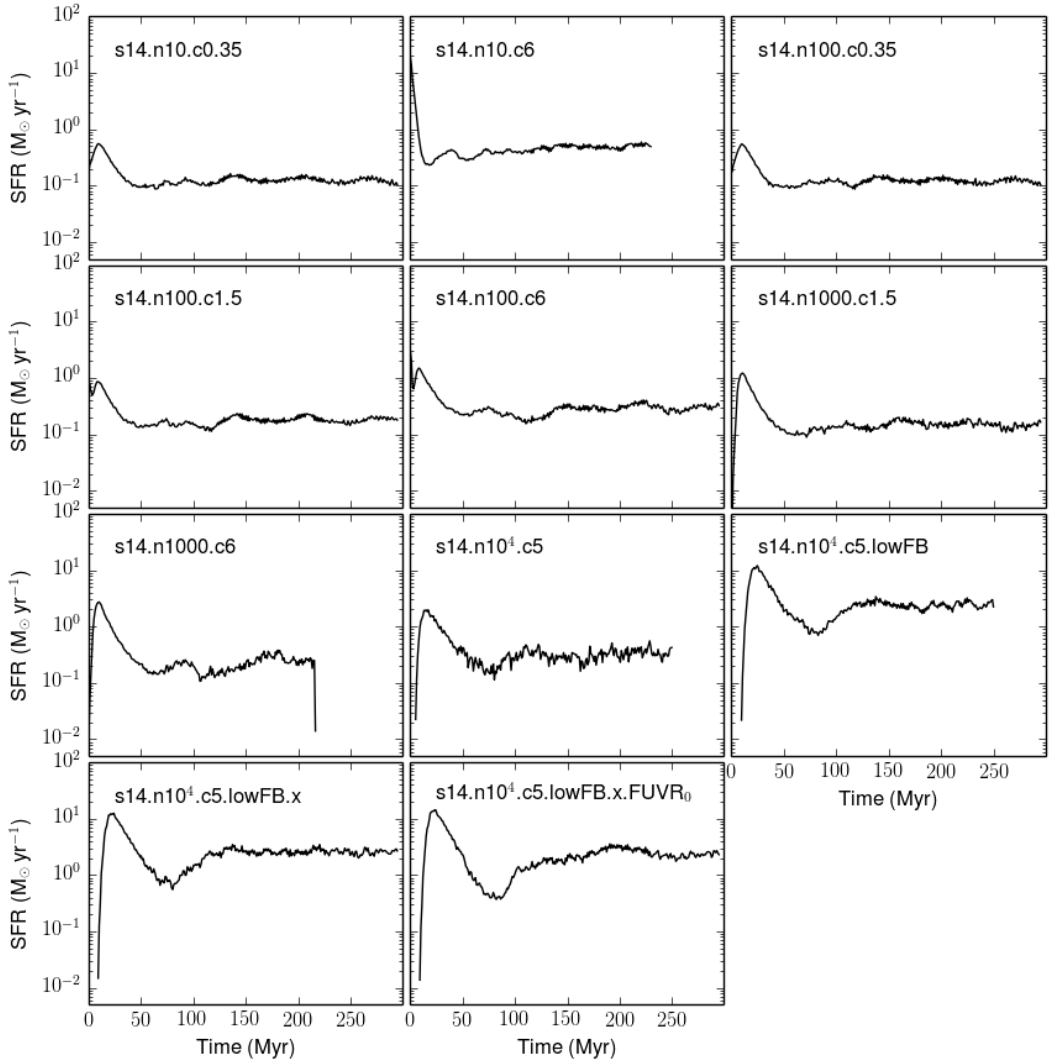

Figure 3.2 The star formation rates for our high surface density discs ($\Sigma_0 = 14$ $M_\odot$ pc^{-2}).

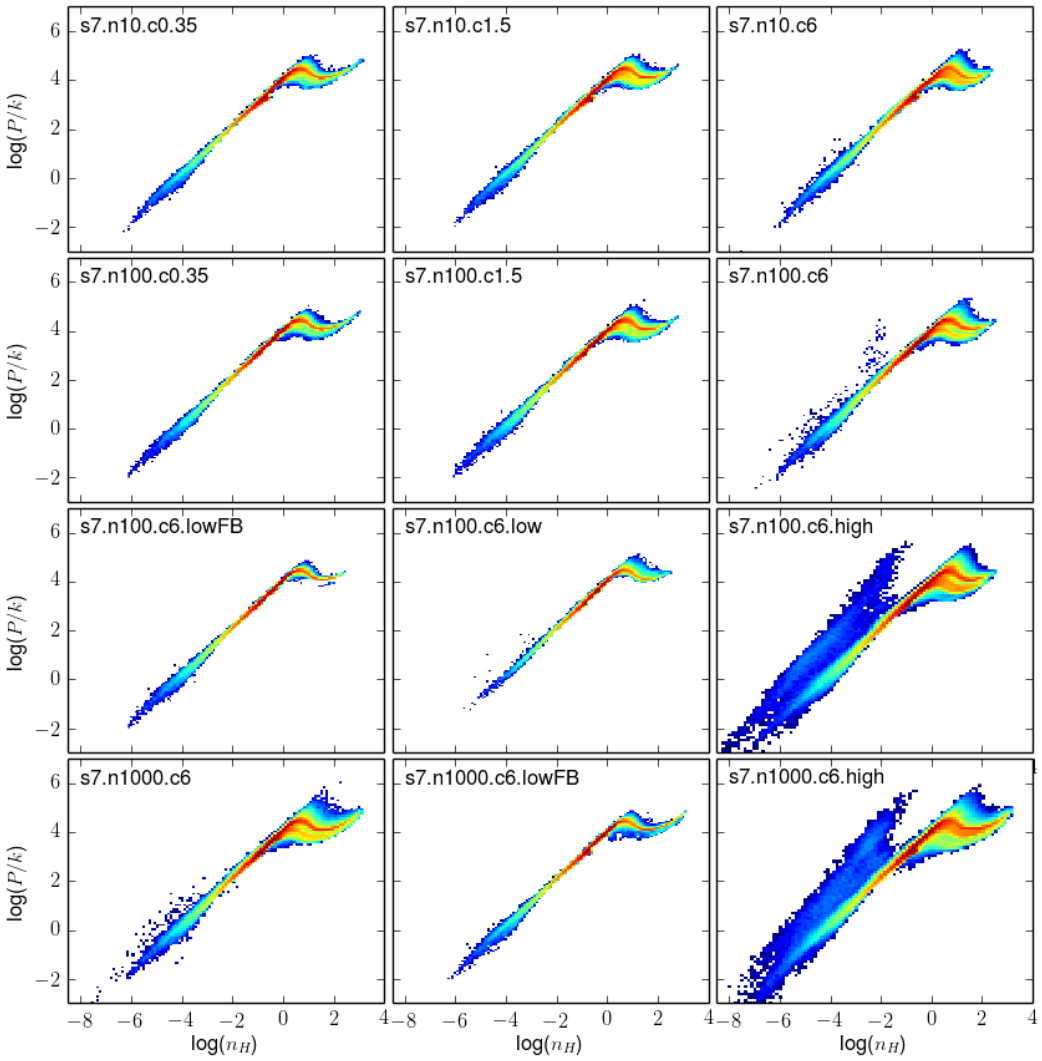

Figure 3.3 Phase diagrams for our low surface density discs ($\Sigma_0 = 7$ M$_\odot$ pc^{-2}).

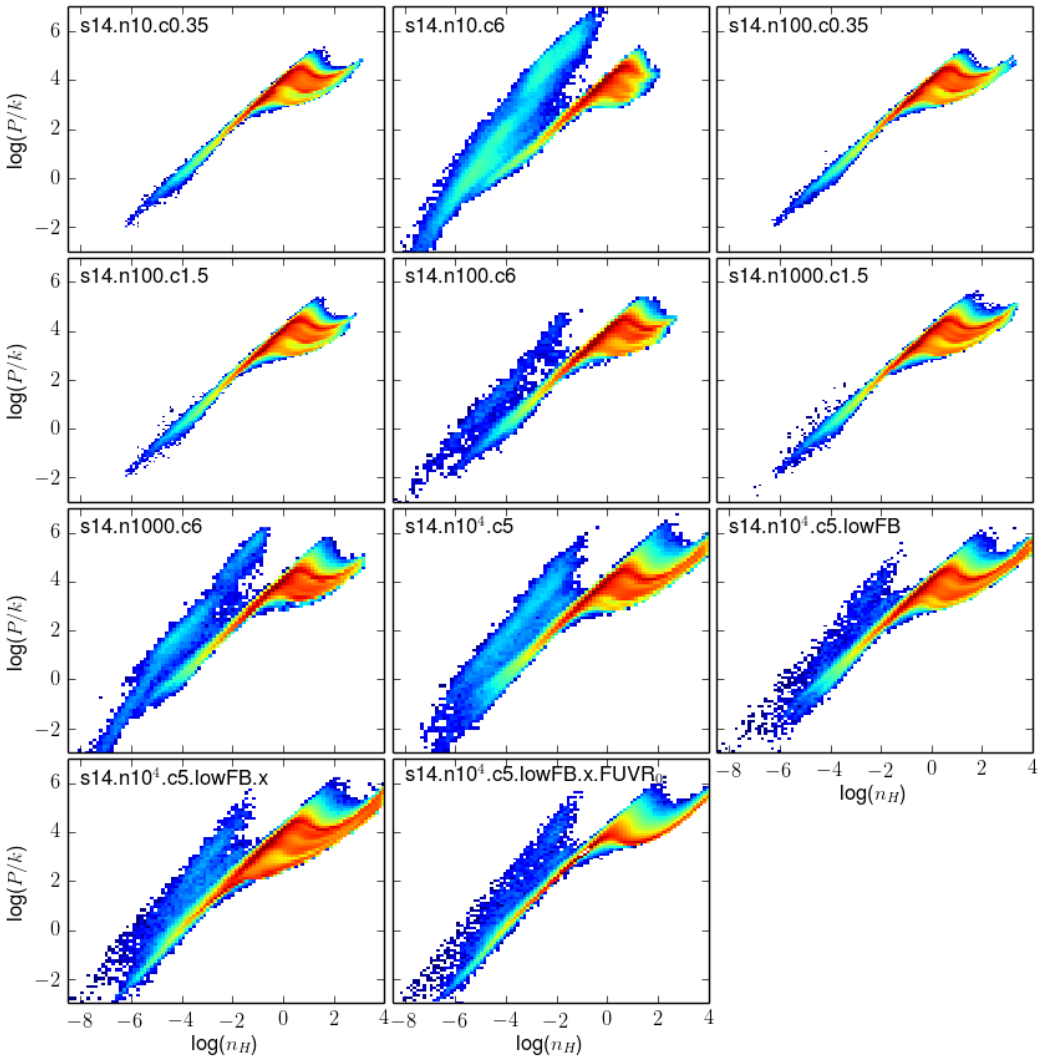

Figure 3.4 Phase diagrams for our high surface density discs (Σ_0 = 14 $M_\odot$ pc^{-2}).

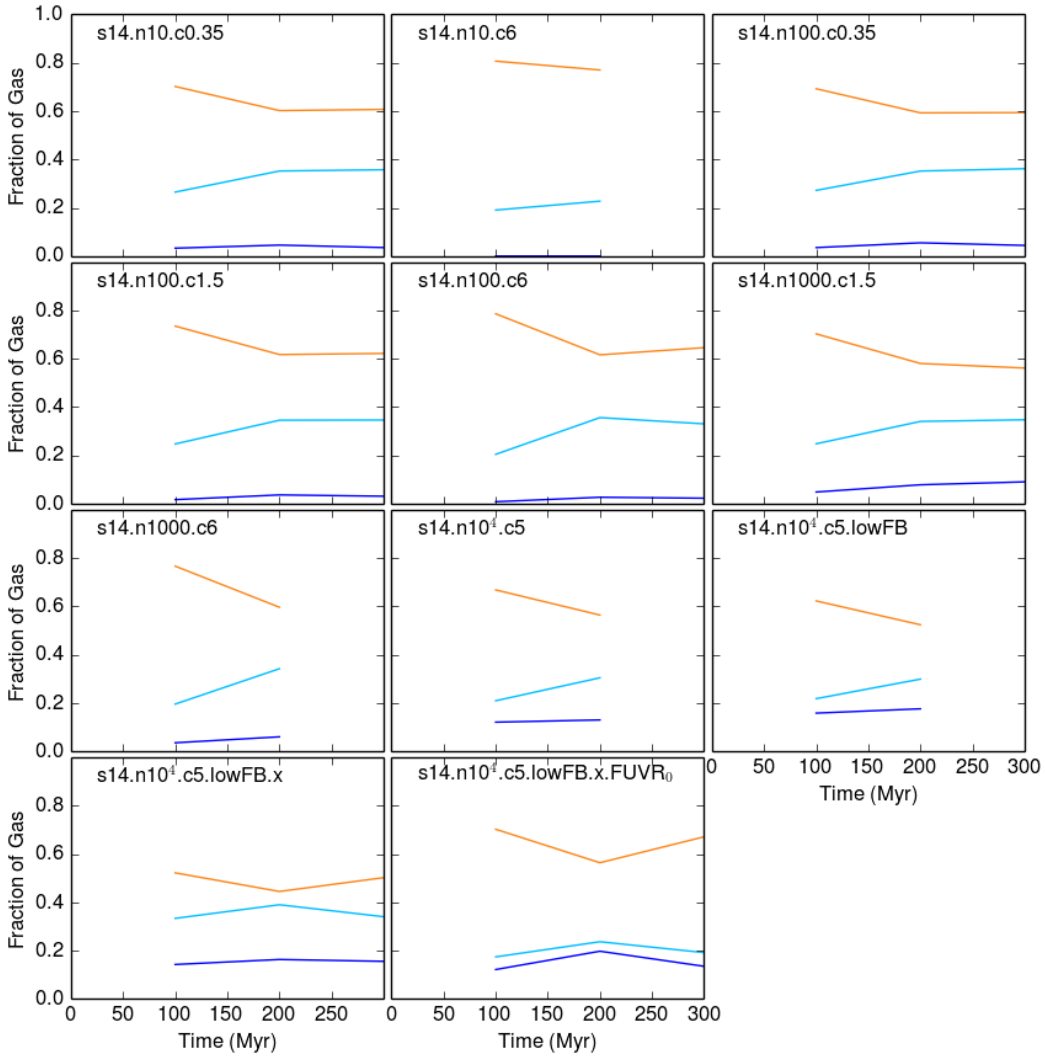

Figure 3.5 Gas fractions for our high surface density discs ($\Sigma_0 = 14$ M$_\odot$ pc^{-2}). Measurements are taken every 100 Myr. The legend is as follows: dark blue - cold gas ($T < 150$ K), light blue - intermediate gas ($150 < T < 5000$ K), orange - warm gas ($5000 < T < 10^5$K).

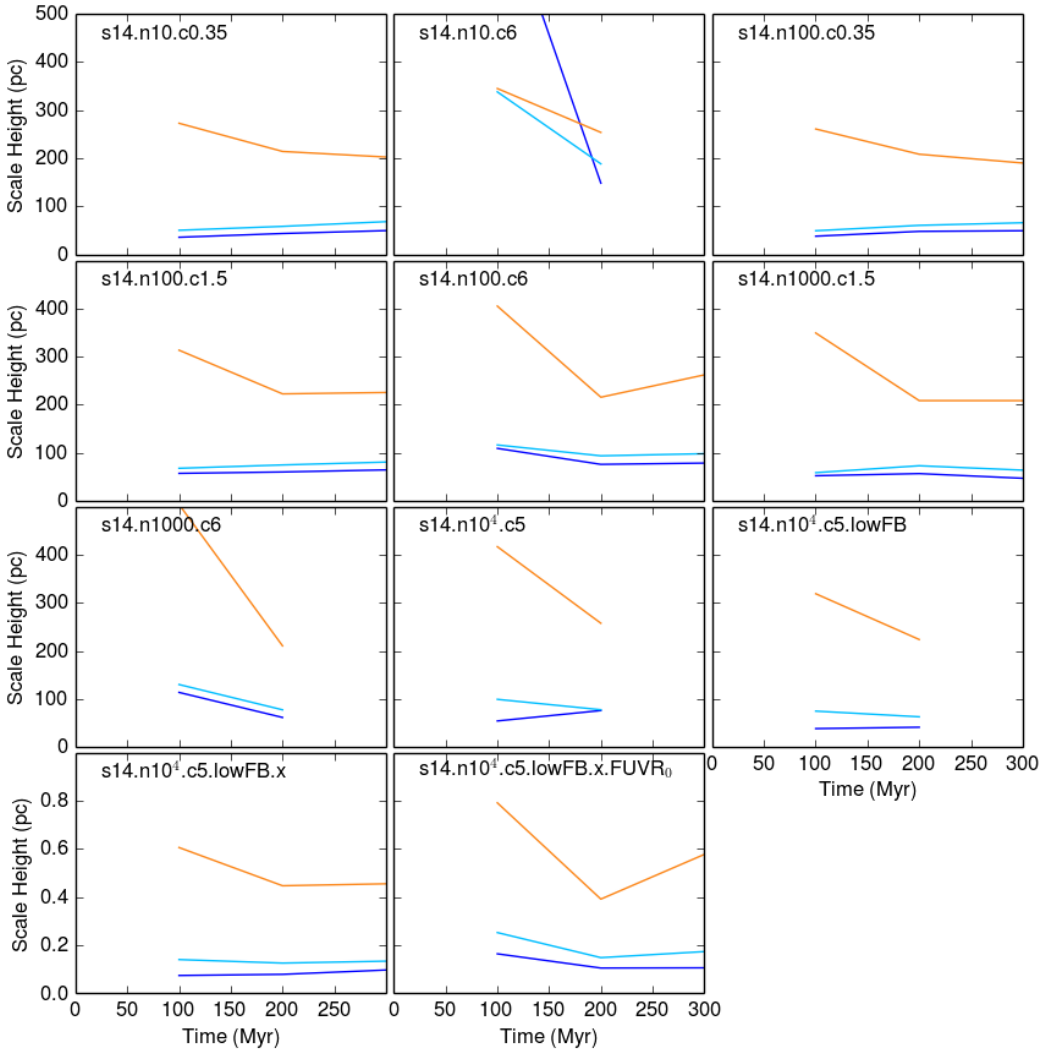

Figure 3.6 Scale heights for our high surface density discs ($\Sigma_0 = 14$ M$_\odot$ pc^{-2}). Measurements are taken every 100 Myr. The legend is as follows: dark blue - cold gas ($T < 150$ K), light blue - intermediate gas ($150 < T < 5000$ K), orange - warm gas ($5000 < T < 10^5$K).

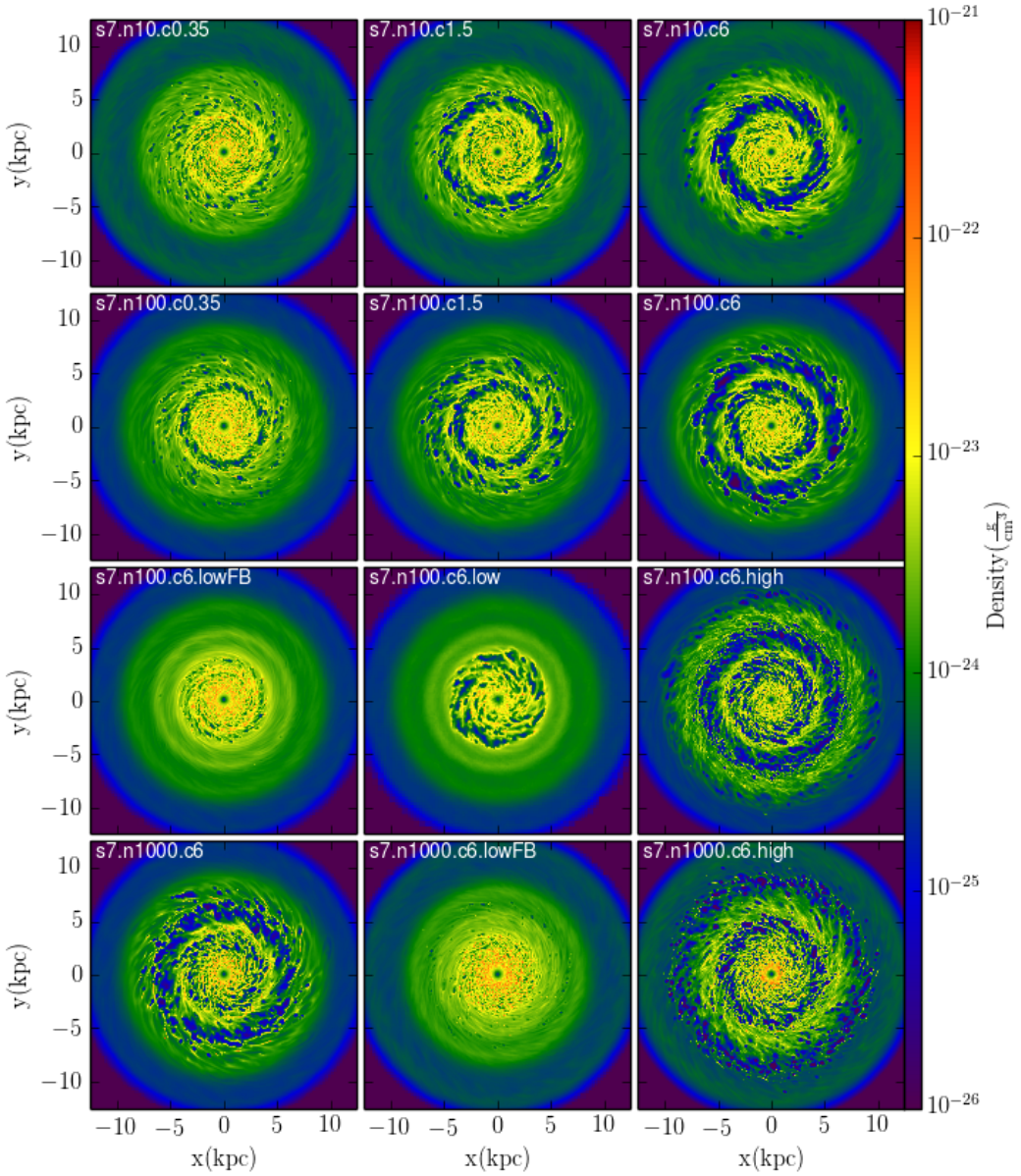

Figure 3.7 Density slices for our low surface density discs ($\Sigma_0 = 7$ M$_\odot$ pc^{-2}).

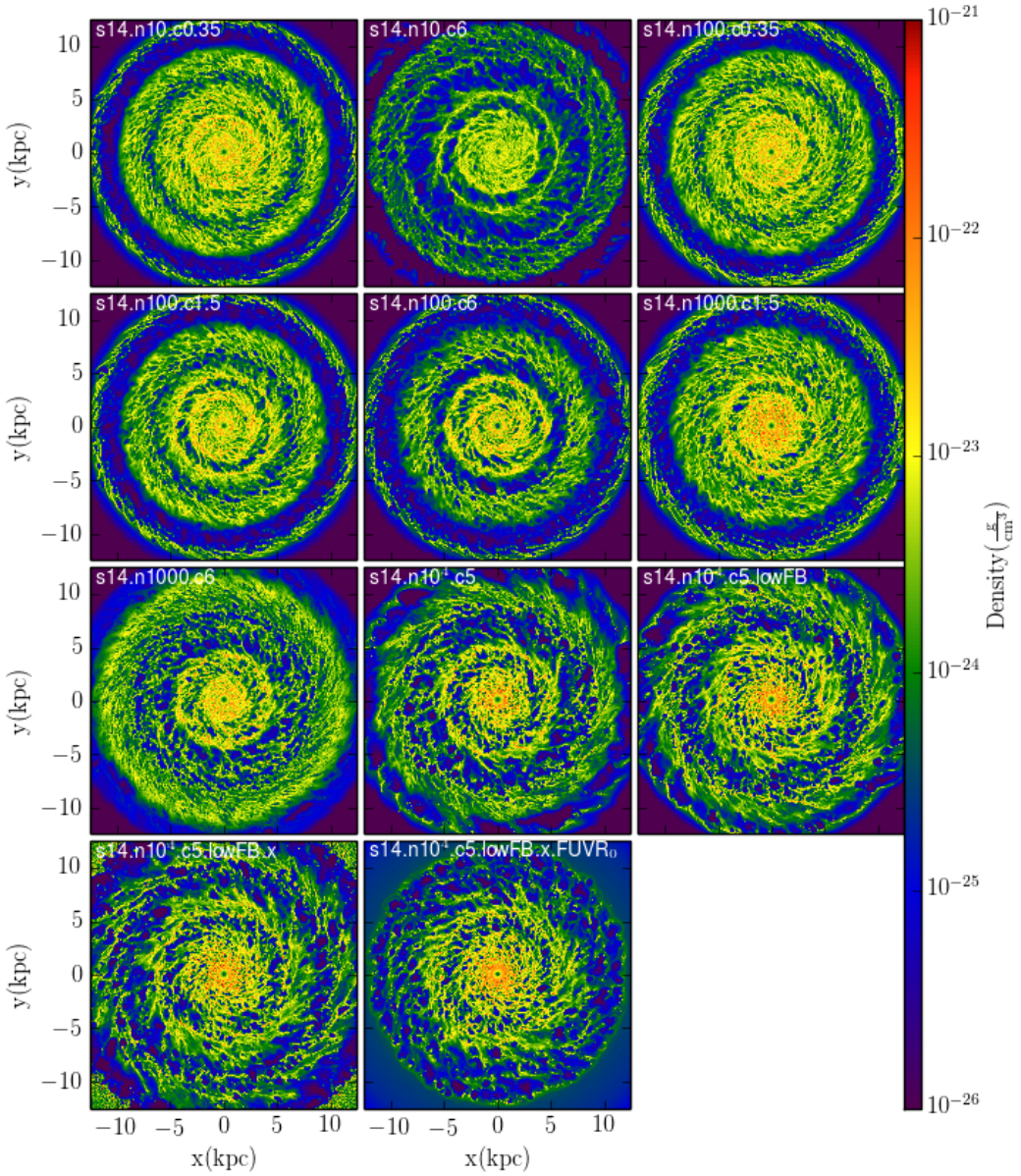

Figure 3.8 Density slices for our high surface density discs ($\Sigma_0 = 14$ M$_\odot$ pc^{-2}).

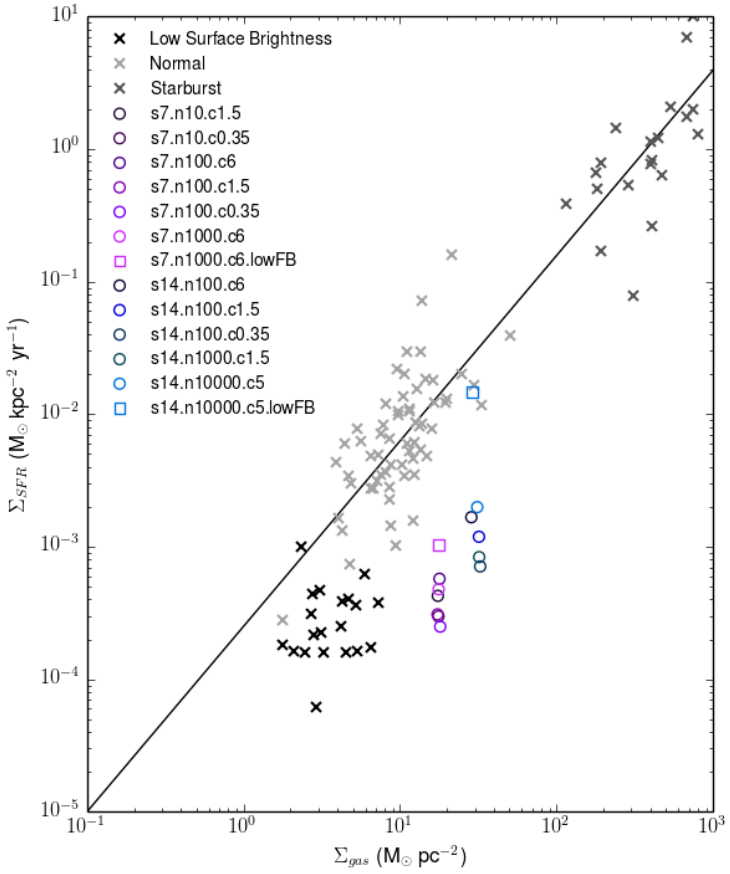

Figure 3.9 The global Kennicutt-Schmidt relation (compare to Figure 1.1). Crosses denote observational data: Black crosses denote LSB galaxies from the sample of Wyder et al. (2009), light and dark grey crosses denote normal and starburst galaxies respectively, both from the original sample of Kennicutt (1998). The black solid line denotes the power-law fit from Kennicutt (1998), $\Sigma_{sfr} \propto \Sigma_{gas}^{1.4}$. The open circles denote our simulations, with open squares representing cases with $\epsilon_{\rm FB} = 10\%$).

3.2 Star Formation: A Self-Regulating Cycle

To begin we explore the claims of Hopkins et al. (2011) that the choice of star formation parameters largely have no effect on the properties of the resulting galaxy. Re-phrased, this suggests that star formation should largely be a self-regulating process where the rate is set by averaged ISM properties. We explore this by varying three star formation parameters: $n_{\rm th}$, c_*, and $\epsilon_{\rm FB}$ and analyzing the impact they have on the global and local state of the disc. As discussed in Section 2.2.1, $n_{\rm th}$ determines the density that a gas particle must exceed to be eligible for star formation, and c_* describes the efficiency with which that eligible gas is turned into star particles. We use $\epsilon_{\rm FB}$ to describe the amount of the available 10^{51} erg that supernovae will inject back into the gas.

3.2.1 Density Threshold ($n_{\rm th}$)

We begin by exploring the impact of the choice of star formation threshold density, $n_{\rm th}$. Choices for this parameter are often motivated by available resolution. As such, it is important to understand the consequences of such a choice. A popular and well motivated choice is, for example, 100 cm^{-3}. This is the average density of GMCs and is a density at which dust grain chemistry allows the efficient formation of molecular hydrogen (Tielens, 2005). Another well-motivated, although still slightly out of reach choice in terms of numerical resolution, would be 10^4 cm^{-3}. This is the density which traces star formation in molecular cores (Lada et al., 2010). Based on these values we explore thresholds between 10 and 10^4 cm^{-3}. Figure 3.10 shows the effect various threshold

choices have on the global star formation rate in the galaxy. In agreement with the findings of Hopkins et al. (2011), changing $n_{\rm th}$ has very little impact on the global star formation rate in both our low and high surface density discs. It should be noted that we are not actually able to reliably resolve a threshold density of 10^4 cm^{-3}, but include it in our study for completeness and to probe behaviour for our eventual goal of increasing the resolution.

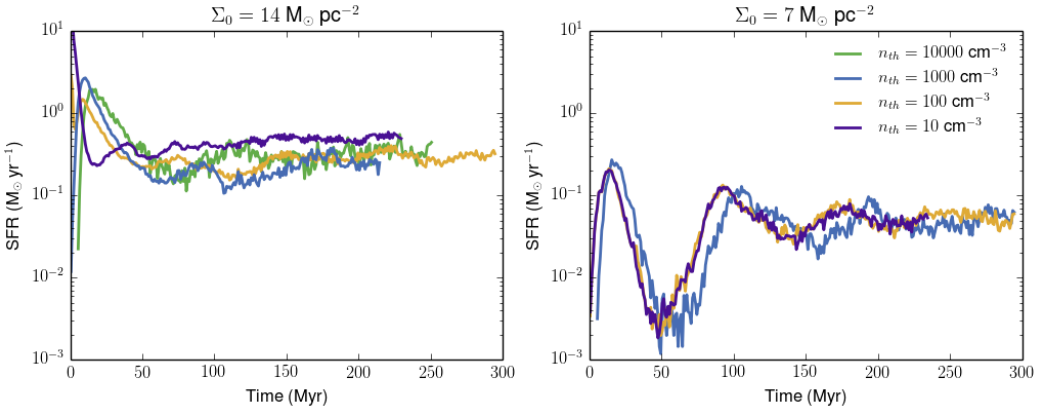

Figure 3.10 The impact of varying threshold density, $n_{\rm th}$ on the star formation rate. For each of the disc, varying $n_{\rm th}$ by four orders of magnitude has minimal impact on the star formation rate.

Based on these findings, one might then conclude that the choice of star formation threshold has little to no impact on the outcome of the simulation. However, what if instead of focusing on global properties, we are interested in local properties and the structure of the ISM? Can we still assume that our choice of threshold will have little impact on the ISM? Figure 3.11 compares the structure of the ISM for simulations s14.n100.c6 and s14.n10^4.c5 (i.e. comparing thresholds of 100 and 10^4 cm^{-3} while holding other parameters ef-

fectively constant), and simulations s7.n100.c6 and s7.n1000.c6. It is now clear that the two cases are not the same.

The top panels of Figure 3.11 show the scale height of each phase of gas (cold, intermediate and warm), while the bottom panels show the fraction of gas in each phase as time in the simulation progresses. For this analysis measurements are taken every 50 Myr. In the case of the low surface density discs (rightmost panels), by 300 Myr the fractions of cold gas are as low as 2.3% and 0.4%. This low fraction makes it difficult to discern valuable information from these cases. We will focus instead on the high surface density discs (leftmost panels). When averaged over later times, once the disc has fully settled, the choice of $n_{\rm th}$ actually has little impact on the scale height. The major difference lies in the fraction of gas in each phase; pushing the threshold to higher densities allows the survival of more of the cold/dense gas phase. In the case of the high density threshold, the fraction of surviving cold gas by a time of 300 Myr is 12.8%, compared to only 2.3% in the low threshold case. These simulations have cold gas scale heights of 78 and 85 pc, for the 100 cm^{-3} and 10^4 cm^{-3} threshold simulations, respectively. In galaxies like the Milky Way, approximately 30% of gas is expected to occupy the cold neutral and molecular phases of the ISM and is expected to have a scale height of $\sim$100 pc (Tielens, 2005). Our fraction of cold gas is lower than expected in for both thresholds. However, in both cases our cold scale height agrees well with that expected.

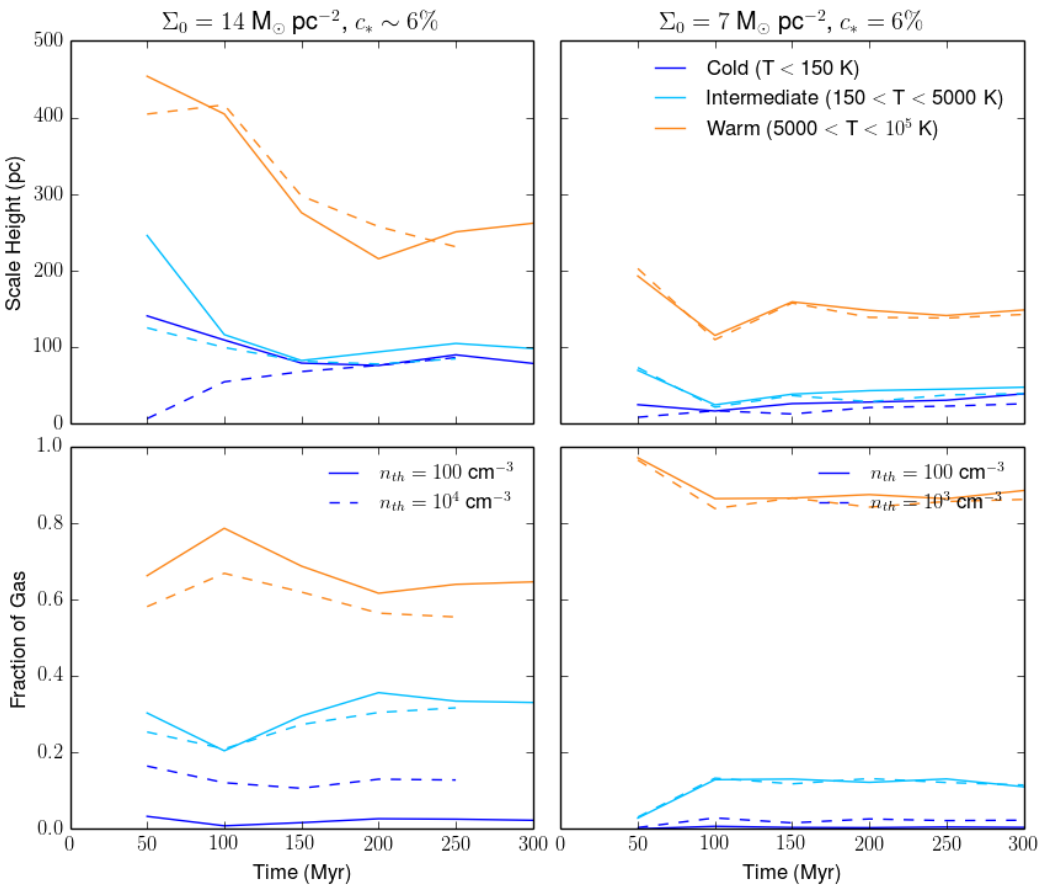

Figure 3.11 Top: the scale height of the gas in each of the three phases. Bottom: the fraction of cold, intermediate and warm. Increasing $n_{\rm th}$ increases the fraction of cold gas in the ISM, but does not have a large effect on the scale height over time, for the high surface density disc.

These differences in the structure of the ISM can be understood by considering the characteristics of star formation in each case. When the threshold is higher, gas must accumulate in dense regions before it becomes eligible to form stars. This leads to different modes of star formation in each case, which can be clearly seen in Figure 3.12. Here, we compare the surface density of

young (age < 100 Myr) stars at thresholds of 10^4 (top panel) and 100 (bottom panel) cm^{-3}. For $n_{\rm th} = 10^4$ cm^{-3}, star formation is very clustered, whereas when $n_{\rm th} = 100$ cm^{-3} the distribution of stars is more diffuse, since more of the gas in the disc is considered eligible. This is seen again in Figure 3.13, which shows zoom-ins of these two snapshots, this time with star particles coloured by their age rather than density. Here it is again clear that for the higher threshold case, star formation proceeds in clustered bursts. These clusters appear to be unbound and we suspect that they drift apart over time. Examples of this drifting can be seen in Figure 3.13. Yellow points denote the youngest stars and dark purple points denote the oldest stars. Yellow points are spatially clustered, while purple points are more spread out. From this we can assume that the stars begin their lives in cluster formations and then drift apart.

Another reason for the extreme clustering in the high threshold case may be due to numerical support. The star formation threshold density in this case is not strictly resolved at our fiducial particle mass. Exceeding the resolution inhibits the ability of gas to collapse further. Thus, if the threshold is too high gas can accumulate at high densities without going on to form stars. This leads to a larger amount of cold/dense gas surviving as compared to other cases.

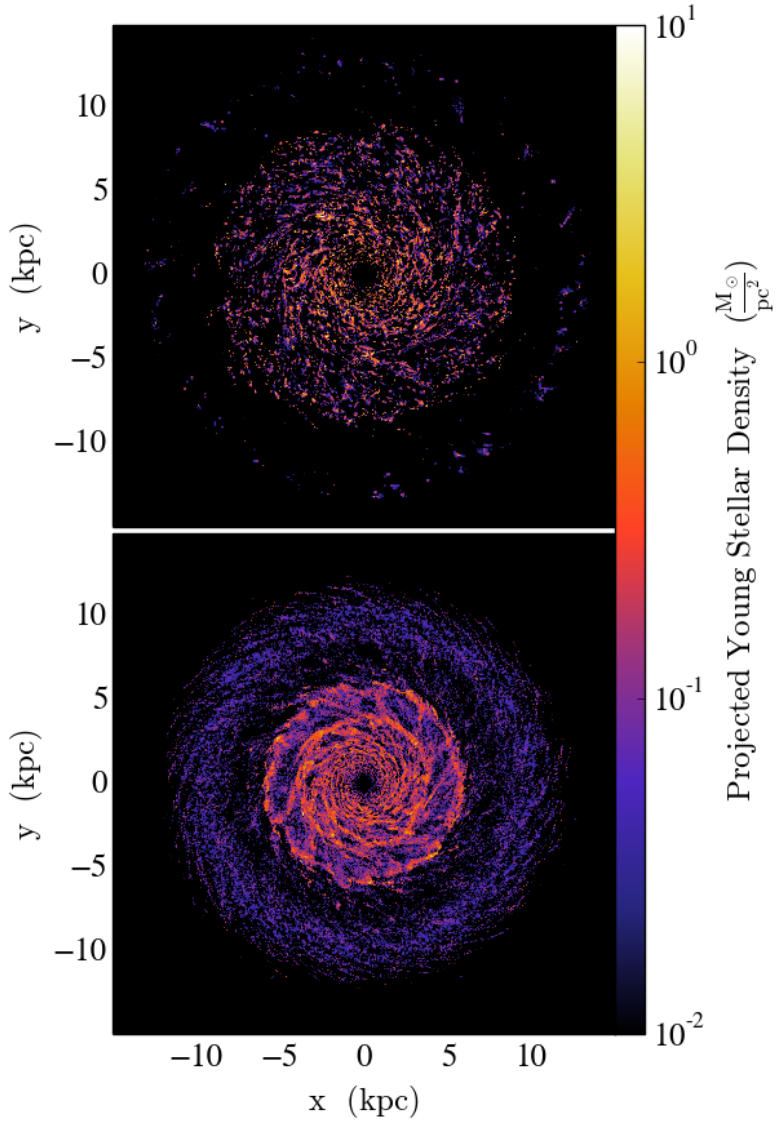

Figure 3.12 The projected density of young stars (age $<$ 100 Myr) at 250 Myr. Top: simulation s14.n10^4.c5. Bottom: simulation s14.n100.c6. When $n_{\rm th}$ is higher, star formation proceeds in a clustered manner. When the threshold is lowered, star formation is permitted to be more diffuse.

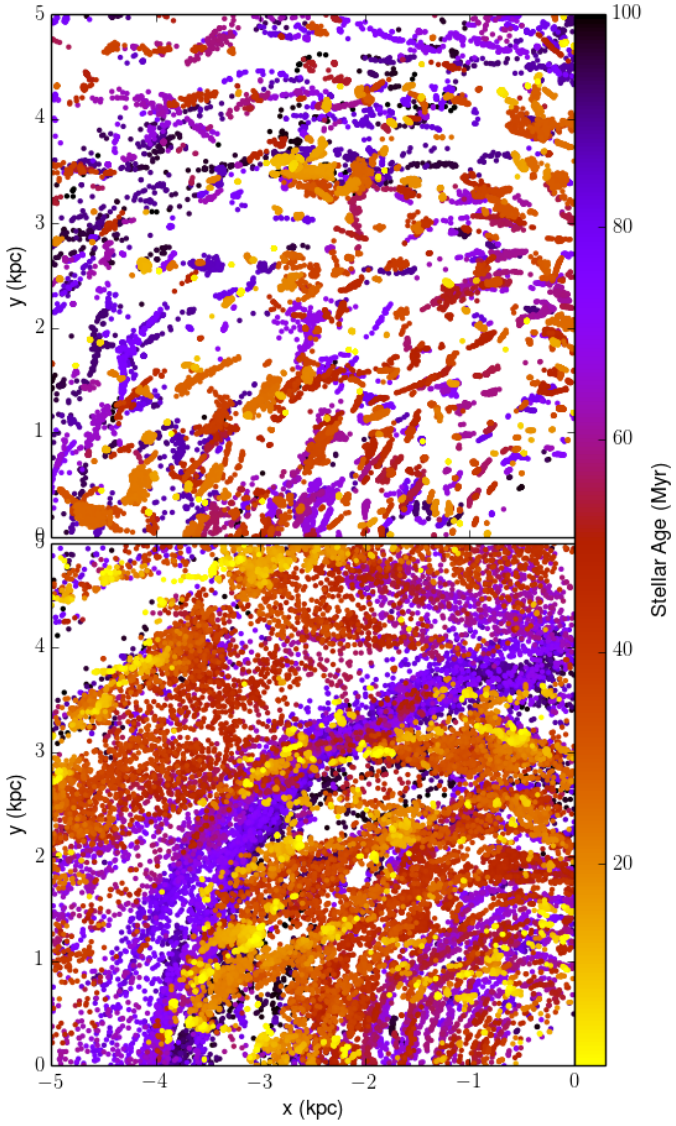

Figure 3.13 A zoom-in of Figure 3.12. Top: simulation s14.n10^4.c5. Bottom: simulation s14.n100.c6. Points represent the positions of individual star particles in the simulation, colour according to their age in Myr. Again, it is clear that when the $n_{\rm th}$ is higher, star formation is more clustered, and when it is lowered, star formation is more diffuse.

3.2.2 Star Formation Efficiency (c_*)

Next, we will look at the impact the choice of efficiency parameter (c_*) for a fixed threshold has on our galaxy. We have explored three different choices for c_*; 0.35%, 1.5%, and 6%. The star formation efficiency in GMCs is inferred to be between $\sim 1 - 2\%$ (Krumholz & Tan, 2007). The high and low end efficiencies are chosen to mirror values used in Hopkins et al. (2011). Figure 3.14 shows the effect that varying this parameter has on the star formation rate (this can also be seen in Figures 3.1 and 3.2). This does have a larger impact than our choice of $n_{\rm th}$. The choice of $n_{\rm th}$ affects which gas particles are tagged as eligible. Rather than changing the amount of eligible gas, varying c_* changes the efficiency with which already eligible gas will be successfully converted to stars. As such we expect that increasing c_* will directly increase the total amount of star formation in the absence of feedback. With regulation by feedback, increasing the efficiency by more than an order of magnitude only increases the global star formation rate by approximately a factor of three.

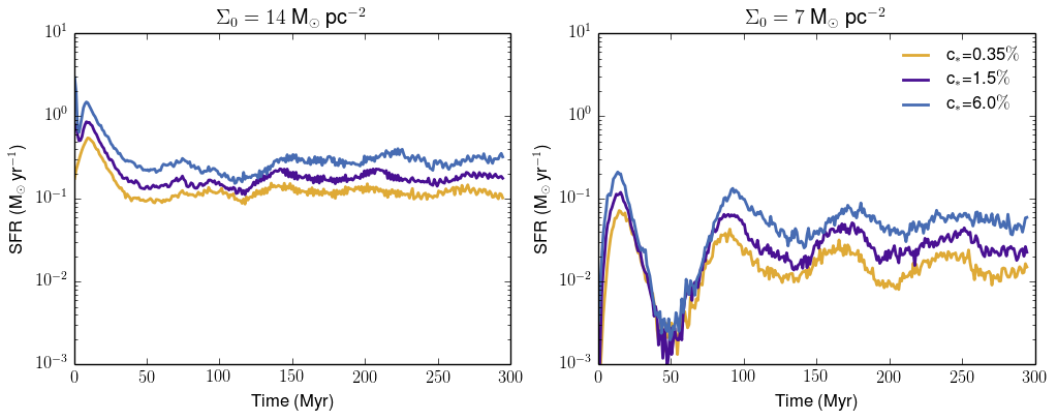

Figure 3.14 The impact of varying star formation efficiency, c_* on the star formation rate. For each of the discs, varying c_* by over an order of magnitude increases the star formation rate by only a factor of 3, approximately

As discussed in Section 3.2.1, this small change in the global star formation rate does not necessarily imply a small change to the local disc environment. Figures 3.15 and 3.16 show density slices through the yz-plane (edge-on) of the disc for simulations s14.n100.c0.35 and s14.n100.c6, respectively. These images are rendered using YT[1], a multi-code analysis toolkit for astrophysical simulations (Turk et al., 2011). YT smooths SPH particles onto grids, which is why the slices appear to have square regions. Large grid sizes indicate regions where there are fewer particles, so the smoothing grid is adjusted to be larger.

[1] Made available to the community at http://yt-project.org/#getyt

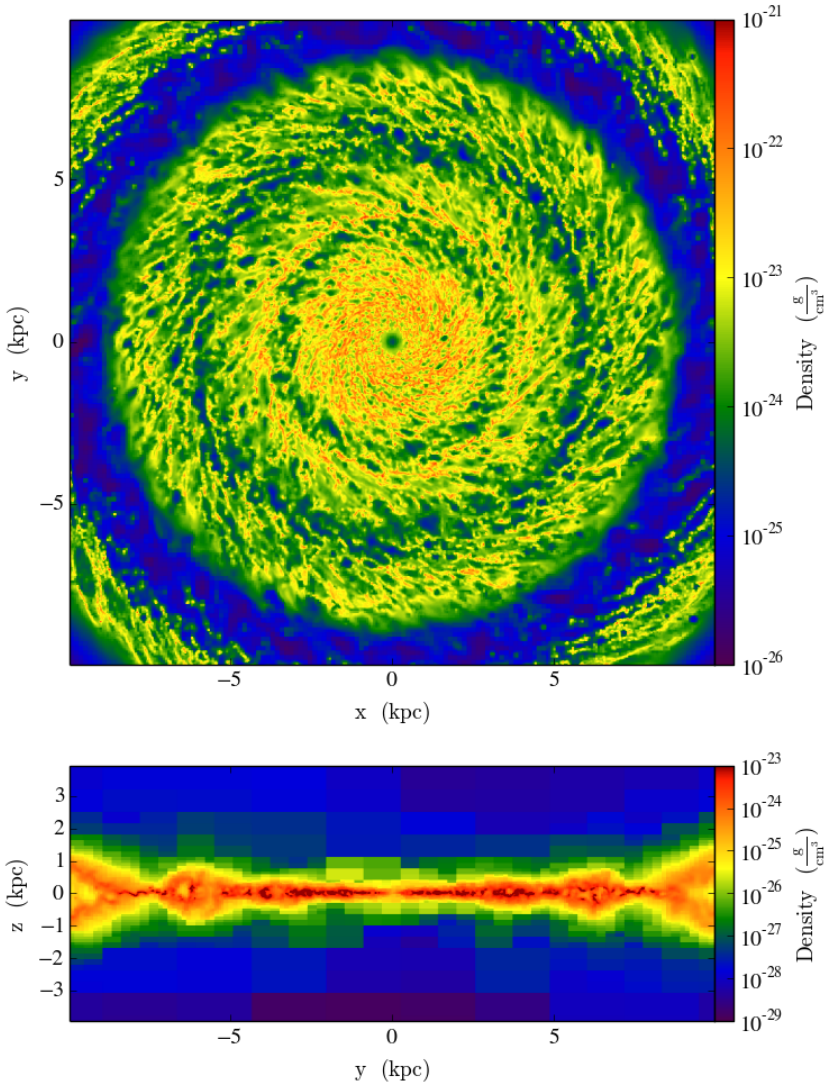

Figure 3.15 Density slices for simulation s14.n100.c0.35 at 300 Myr. Top: a slice through the center of the xy-plane of the disc. Bottom: a slice through the center of the yz-plane of the disc.

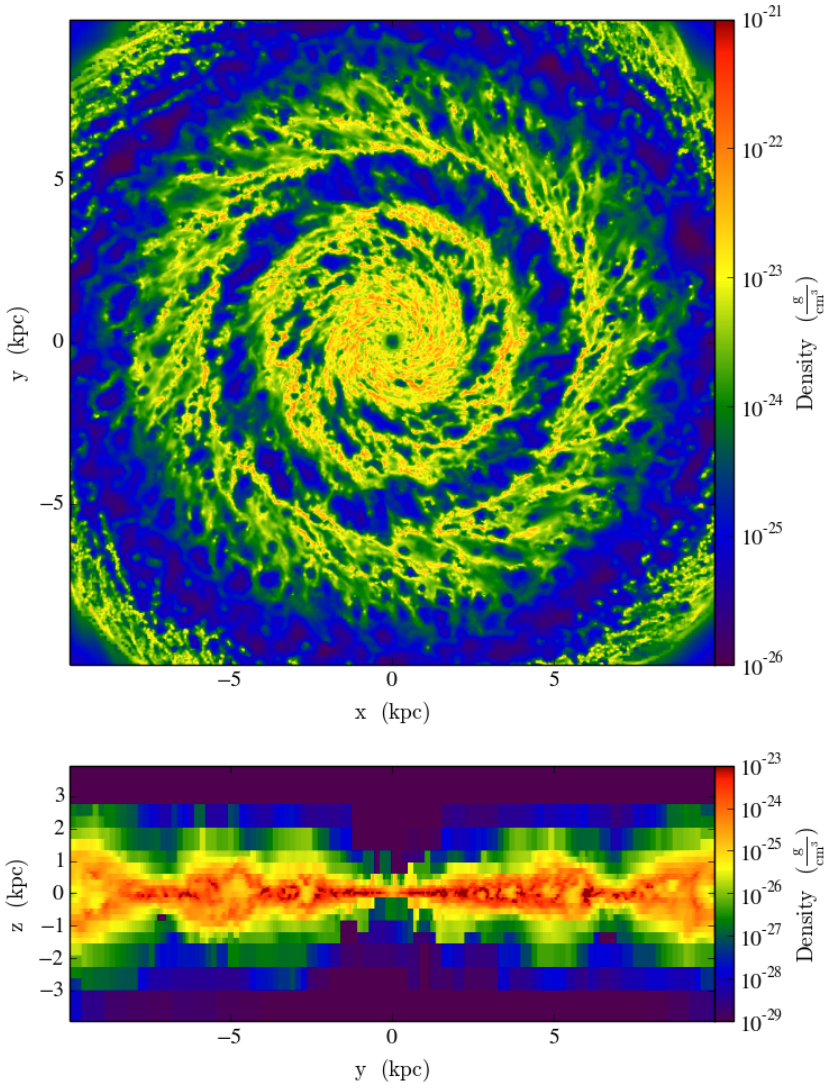

Figure 3.16 Density slices for simulation s14.n100.c6 at 300 Myr. Top: a slice through the center of the xy-plane of the disc. Bottom: a slice through the center of the yz-plane of the disc.

The biggest difference here is the height to which the gas extends above each of the discs. Increasing c_* appears to have a large impact on the scale height of the galaxy. This is confirmed by plotting the scale height, shown in

Figure 3.17. Here the scale height and gas fractions are plotted for both cases in the high and low surface density discs. Again, since the cold fraction in the low surface density discs are so low, 2.3% and 0.83% for c_* of 6% and 0.35%, we will focus on the high surface density cases. We find that increasing c_* by an order magnitude decreases the fraction of cold gas from 4.4% to 2.3%.

We speculate that this can be understood by considering the pressure in the disc. Star formation is driven to an equilibrium state. Increasing c_* increases the amount of stars formed, increasing the total effective pressure. This is balanced by an increase in the scale height, which increases the gravity felt throughout the disc ($P = \int \rho g \, \mathrm{d}z$). Focusing again on the cold gas, increasing c_* from 0.35% to 6%, increases the average scale height from 49.6 to 78.5 pc. Although there is an increase, it is modest, and does not exhibit a one-to-one correlation with the increase in star formation.

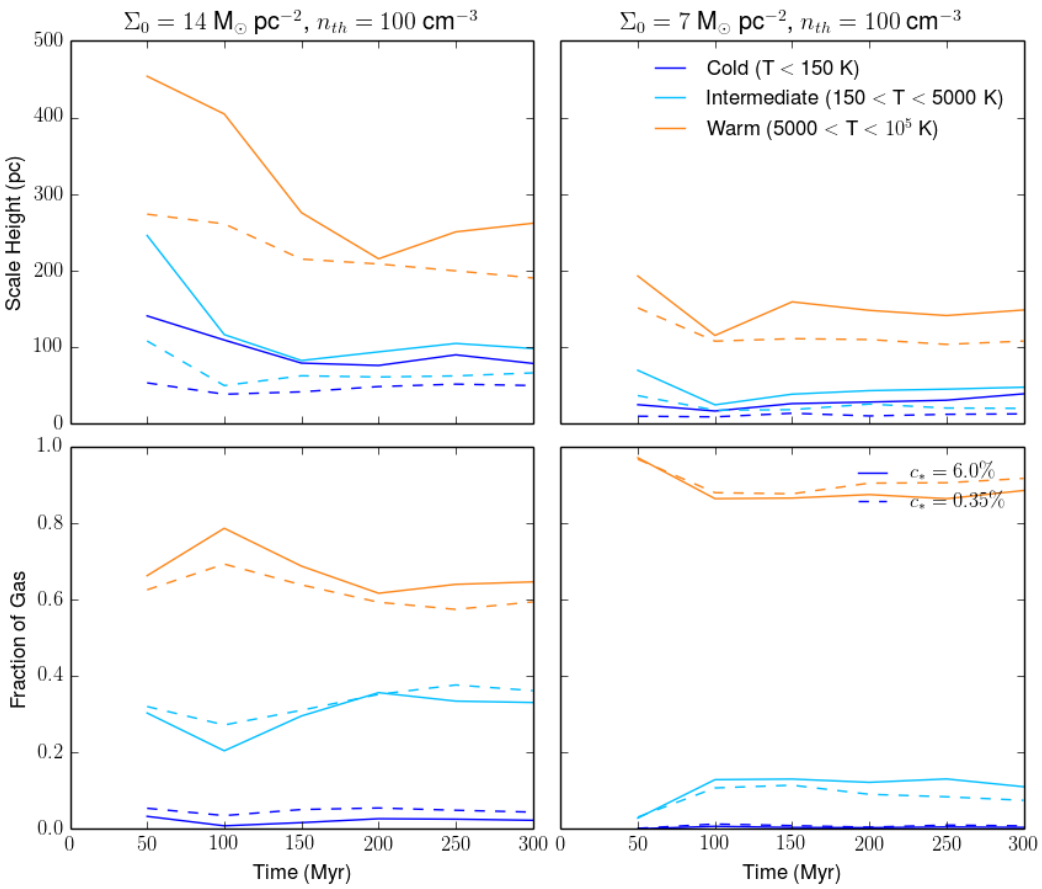

Figure 3.17 Top: the scale height of cold, intermediate and warm gas. Bottom: the fraction of the gas in each of the three phases. Increasing c_* significantly increases the scale height in all three temperature ranges, in the case of the high surface density disc.

3.2.3 Supernovae Feedback Efficiency (ϵ_{FB})

We have now looked at two parameters which appear to have little effect on the global star formation rate, but have important consequences for the ISM. The last parameter we have considered is the feedback efficiency, ϵ_{FB}. We

have contrasted two choices for this parameter 100% and 10%, corresponding to supernovae injection energies of 10^{51} and 10^{50} erg, respectively. Again, we start by examining the global star formation rate, plotted in Figure 3.18 (and also in Figures 3.1 and 3.2). Unlike previous cases, we find a large difference in the global star formation rate when varying $\epsilon_{\rm FB}$. As well, the amount of this impact is affected by the choice of the other star formation parameters and the chosen initial conditions. In the high surface density case, lowering feedback efficiency lowers the amount of energy injected by supernovae, and in turn increases the star formation rate by an order of magnitude. In this case, star formation is clustered, and so stars work together making feedback extremely effective at heating gas. In the low surface density discs we do not see a decrease in feedback efficiency being accompanied by an increase in the star formation rate. Comparing simulations s7.n100.c06 and s7.n100.c06.lowFB (in Figure 3.1) and s7.n1000.c6 and s7.n1000.c6.lowFB (in Figure 3.18, changing $\epsilon_{\rm FB}$ leaves the star formation rate unchanged.

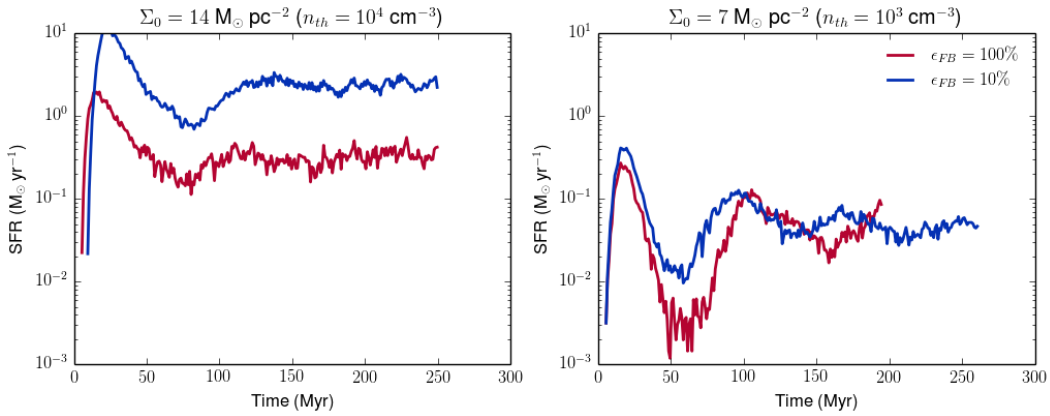

Figure 3.18 The impact of varying star formation efficiency, $\epsilon_{\rm FB}$ on the star formation rate. Varying the feedback efficiency is not as straight-forward as varying the other parameters, its behaviour is non-linear with respect to the other choices, and even the choice of initial disc setup.

Figure 3.19 shows scale height and gas fractions, while Figure 3.20 shows phase diagrams for the two simulations from Figure 3.18. Here we see that in low surface density discs, almost all of the gas lies along the equilibrium curve. As we have already discussed, the star formation rate in the disc will regulate itself to the pressure. In the low surface density discs the star formation rate is low. In principle, these stars inject pressure into the disc through feedback. However, considerable thermal pressure support is injected by our radially varying photoelectric heating term. Since this term is not directly coupled to actual star formation in the simulation, it creates a base thermal pressure everywhere in the disc. The thermal and turbulent pressure injected by feedback from stars will not be larger than the background thermal pressure from photoelectric heating in the low surface density discs. Thus we see

a smaller impact being made by the lowered feedback efficiency. This is illustrated in Figure 3.21. For high surface density discs, the turbulent pressure dominates the thermal pressure by an order of magnitude. Thus, the regulation of star formation via the effective pressure can be heavily influenced by the amount of feedback energy injected. If we look instead at the low surface density disc this is no longer the case. Turbulent pressure does not dominate the thermal pressure. Particularly in the low feedback efficiency case, it is the thermal pressure that sets the effective pressure and thus will regulate star formation. This implies that changing the feedback efficiency will have little to no effect on the star formation rate.

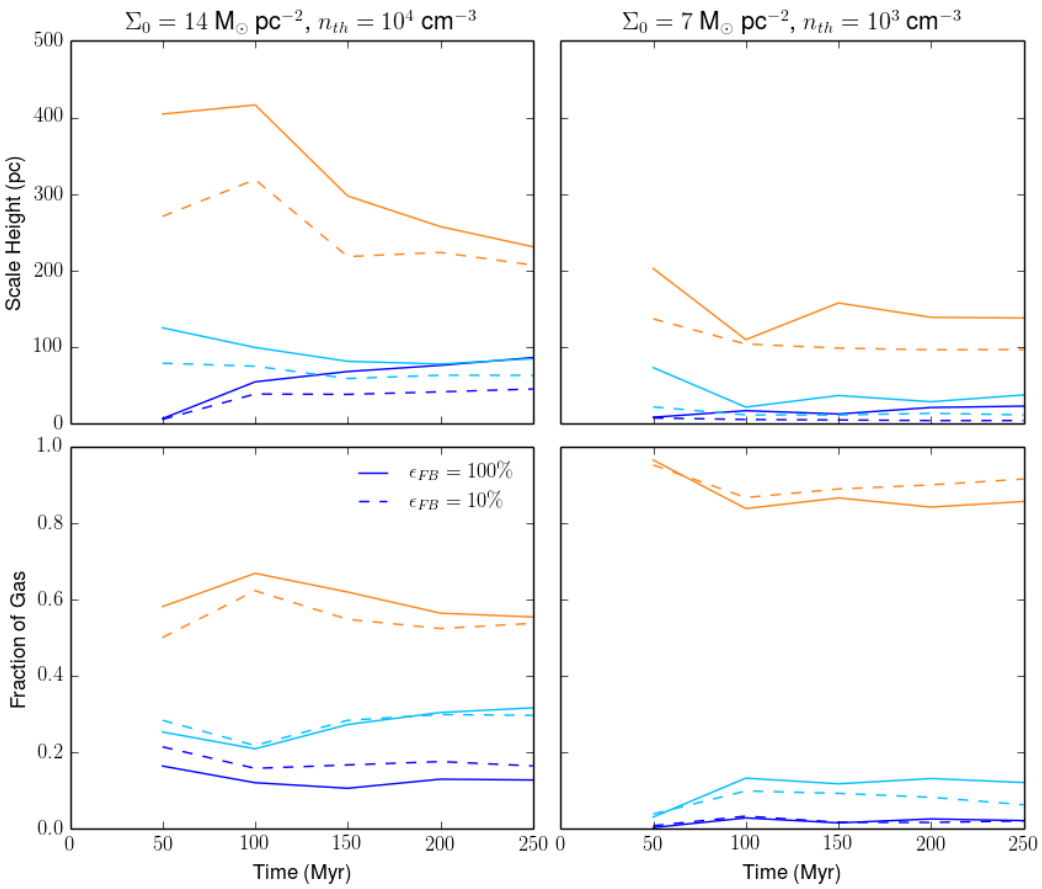

Figure 3.19 Top panel: Fraction of cold, warm and hot gas. Bottom panel: Scale height. Varying $\epsilon_{\rm FB}$ has a small impact on both the fraction of gas in each phase and the scale height of the gas.

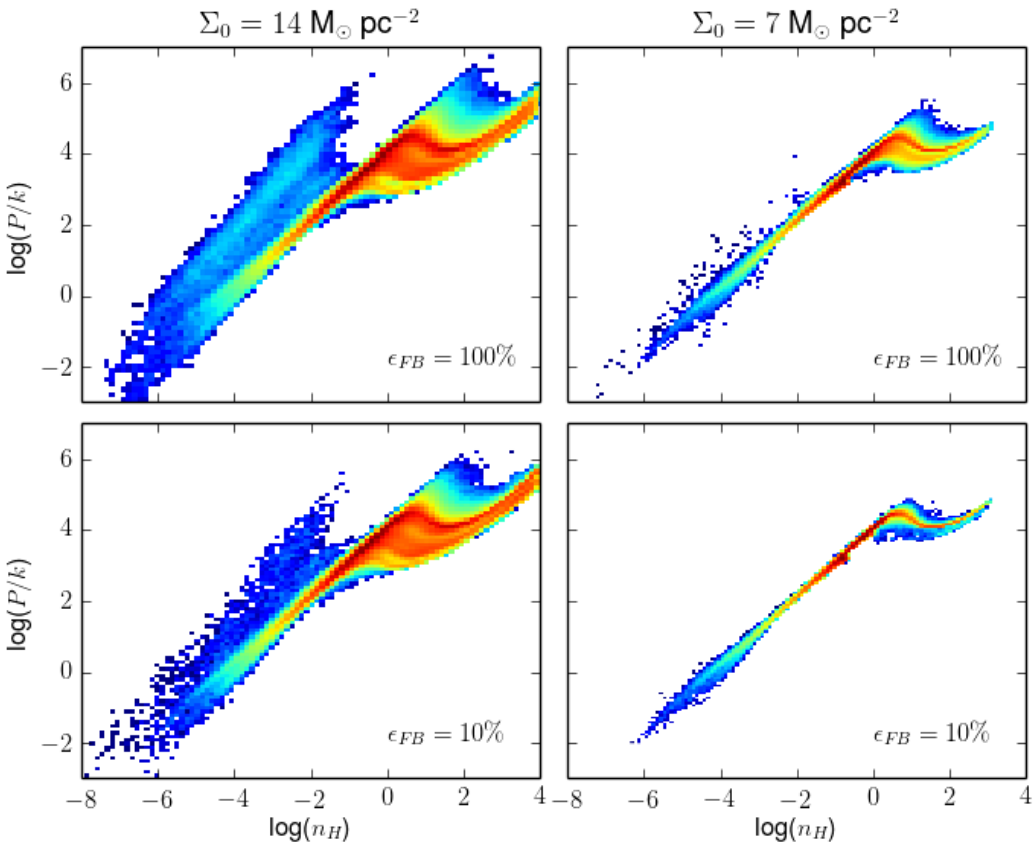

Figure 3.20 Phase diagrams for discs with varying $\epsilon_{\rm FB}$. Changing the feedback efficiency is not as straight forward as changing the other parameters; its behaviour is non-linear with respect to the other parameter choices, and even the choice of initial disc setup.

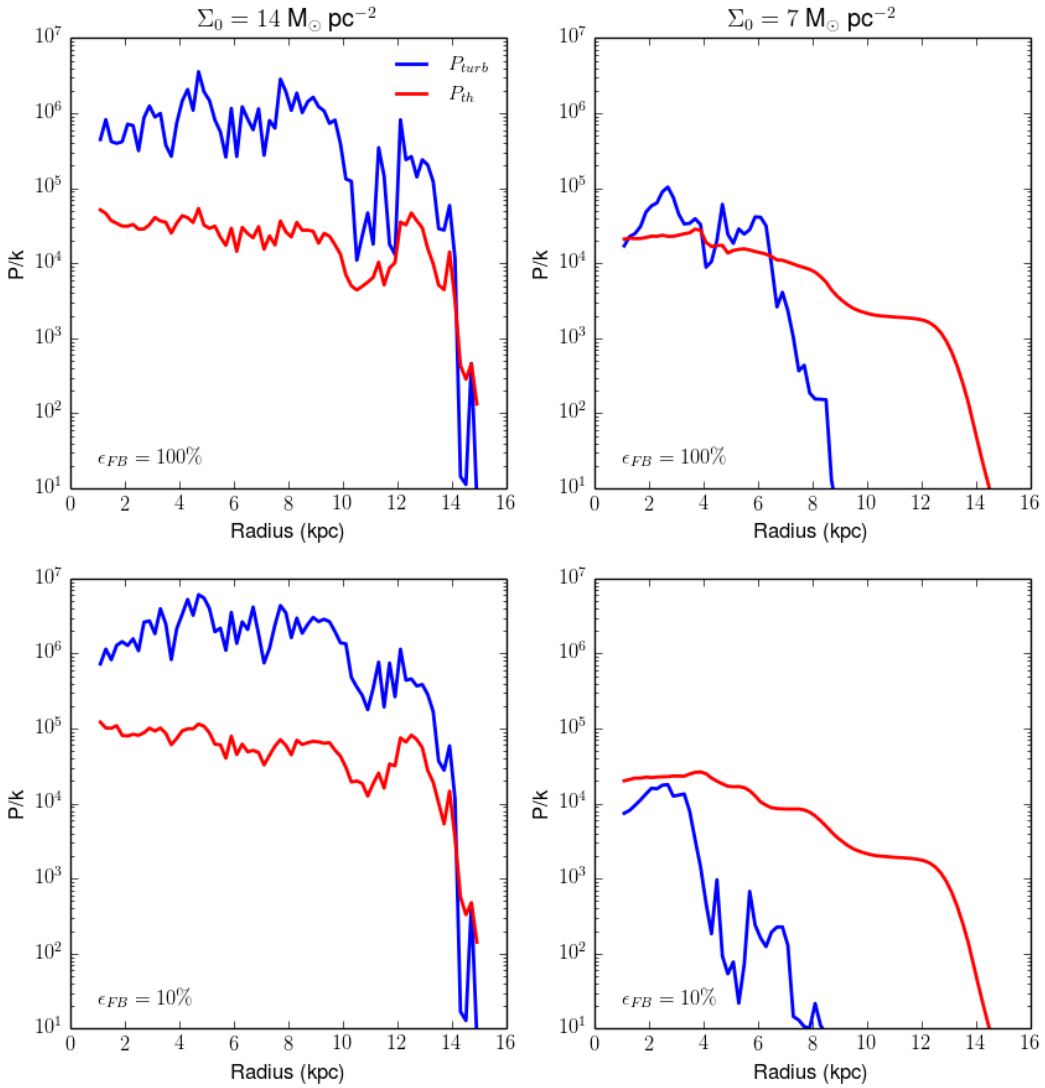

Figure 3.21 Radial pressure for the two discs in Figure 3.20. The red line denotes the average thermal pressure, P_{th}, and the blue line denotes average turbulent pressure, P_{turb}.

3.2.4 A Resolution Study

We have completed a resolution study to check for convergence at our fiducial resolution (with particles mass of 441.94 $M_\odot$). We choose simulation s7.n100.c6 for this comparison. The choice of a lower surface density disc is motivated by particle number; a lower surface density means fewer particles at the fiducial resolution, implying we can increase the particle mass without unmanageable computing slow-down. As such, we have re-run this simulation at lower resolution with a particle mass of 3535.53 $M_\odot$ (s7.n100.c6.low) and at higher resolution with a particle mass of 55.24 $M_\odot$ (s7.n100.c6.high).

Figure 3.22 shows density projections of the discs at 100, 200 and 300 Myr of evolution. The ring structure is much more prominent in the high resolution disc. Figure 3.23 shows the global star formation rates, phase diagrams, gas fractions, and scale heights for these discs. We see that the star formation rate converges to approximately the same rate of 0.05 $M_\odot$ yr^{-1} by 300 Myr. Also, as we increase the resolution we increase both the fraction and the scale heights of the cold and intermediate gas. We also see more turbulence as we increase the resolution (as seen in the phase diagrams). At high resolution the phase diagram is much more spread out; gas does not hug tightly to one equilibrium curve as it does in the lowest resolution simulation.

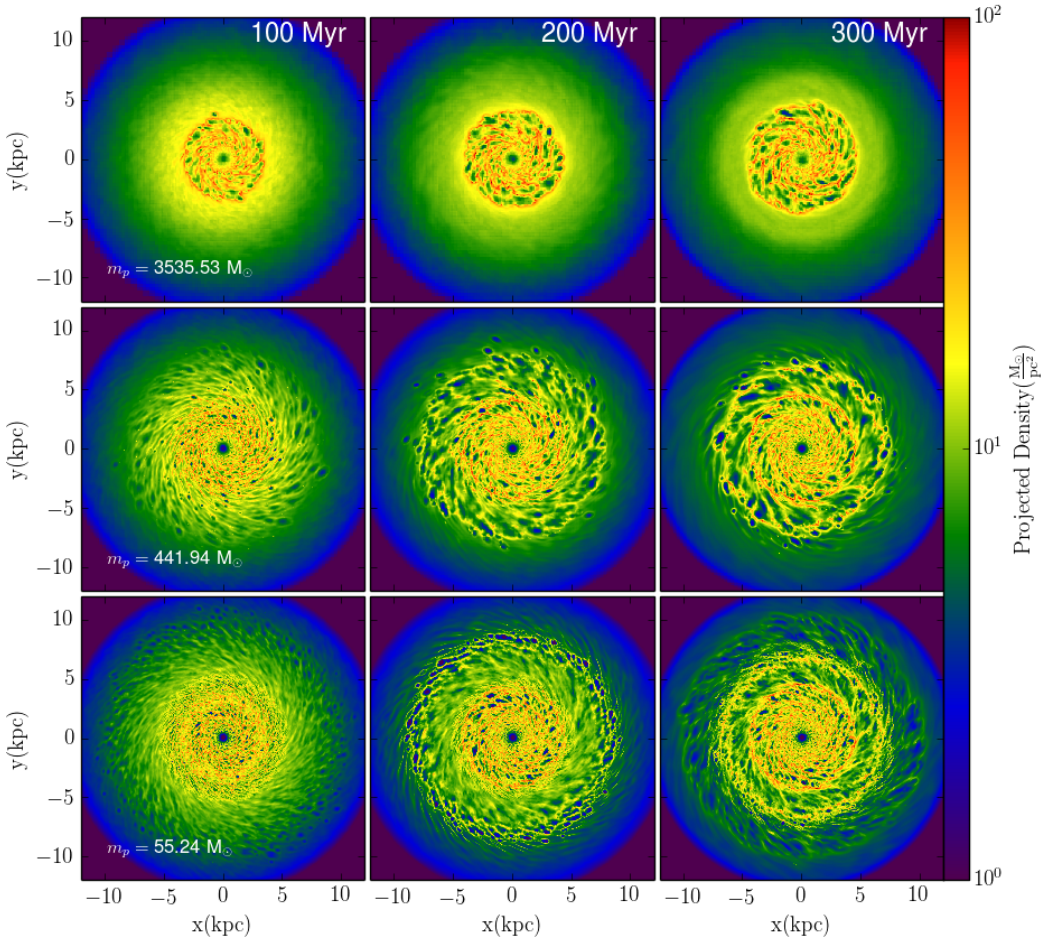

Figure 3.22 Density slices through the xy-plane of the disc (resolution increases downward).

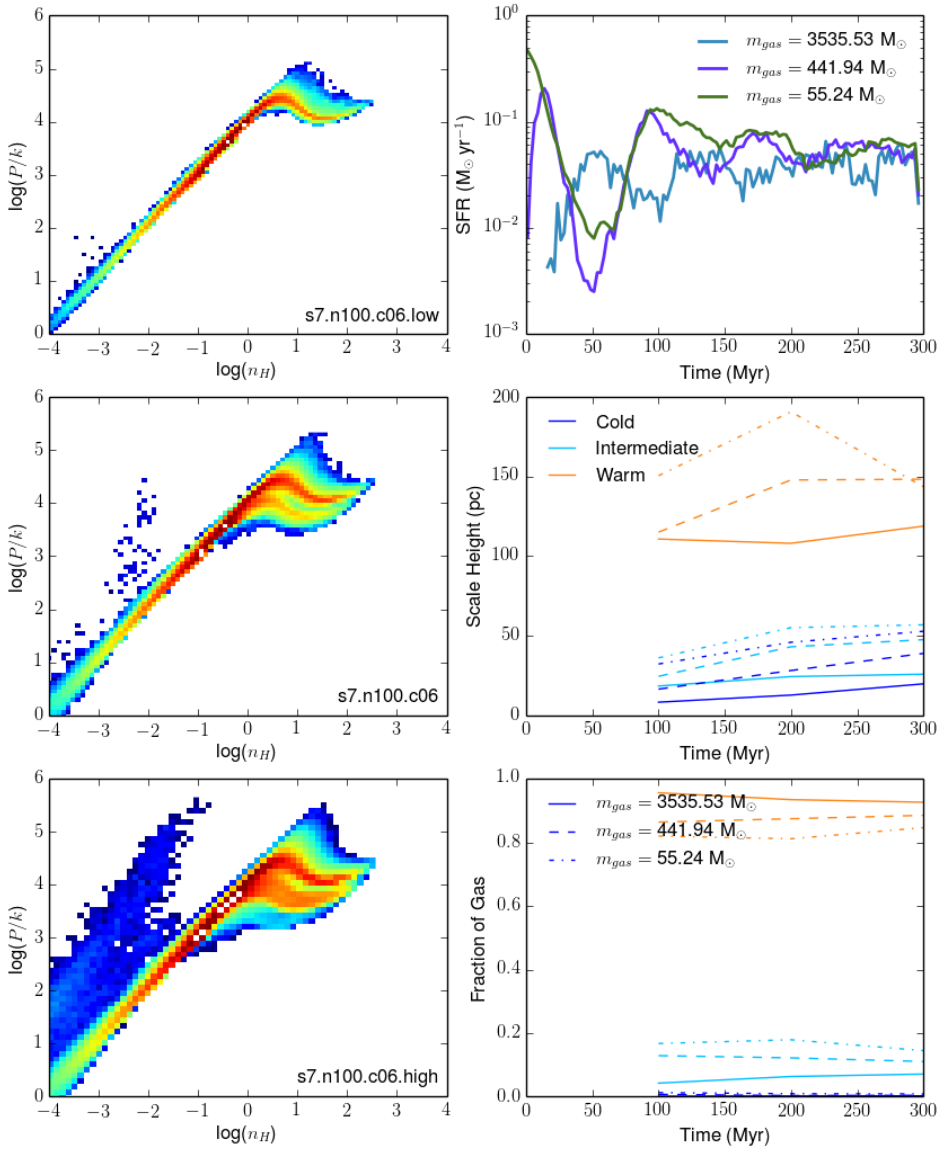

Figure 3.23 Properties of the ISM for the simulations included in the resolution study. Left panels: phase diagrams, with simulation resolution increasing downward. Top right panel: Star formation rate for the three different resolutions. Middle right panel: Scale height for each phase of gas in each of the three simulations. Bottom right panel: fraction of gas in each phase.

3.3 The Correlation Between Pressure and Star Formation

We can now use our suite of simulations to explore other ideas. Of particular interest is the effect that our newly implemented two-phase model has on the truncation of star formation in the disc. What we are seeking to confirm or deny is whether it is the disappearance of the two-phase instability in the outer regions of the galactic disc that causes star formation to stop. Figure 3.24(a) shows the results of such a calculation for simulation s7.n100.c1.5. Here the thermal pressure is shown in red, the turbulent pressure in blue and the total pressure ($P_{\rm th} + P_{\rm turn}$) in black (dashed). Plotted as filled circles are average thermal pressures from Wolfire et al. (2003); these represent the average thermal pressure required to maintain a two-phase medium (error bars indicate min/max). The star formation rate surface density ($\Sigma_{\rm SFR}$) is plotted in the lower panel. Immediately obvious is that the turbulent pressure traces the star formation (this makes sense since stars create turbulence via stellar feedback). In the case of this disc, the star formation is truncated at a radius of approximately 8 kpc. Shown in Figure 3.24(b) is the phase diagram for gas in 2 kpc thick radial annuli. A definite two-phase structure is present in the plots until a radius of 8 kpc, corresponding to the location in the disc where the star formation is truncated.

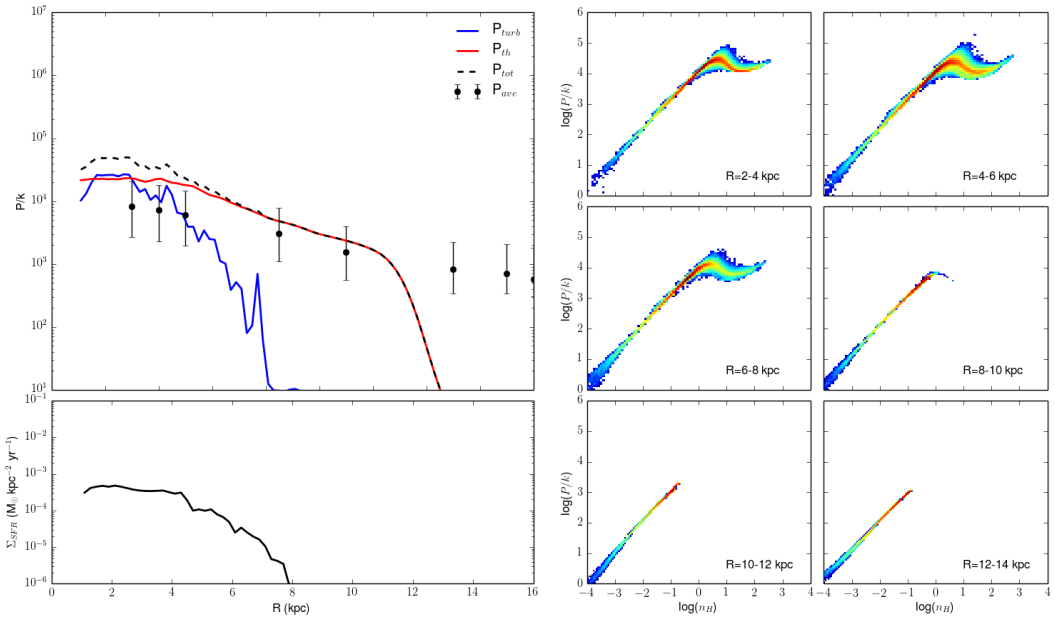

Figure 3.24 ($\Sigma_0 = 7$ M$_\odot$ pc^{-2})Total, thermal and turbulent pressure averaged for rings through the xy-plane of the disc. Points represent the average thermal pressure required produce a two phase medium (Wolfire et al., 2003). This is compared to phase diagrams for the disc at various radii. The fall-off in $\Sigma_{\rm SFR}$ corresponds well to the location in the disc where there is no longer a two-phase medium (between 8-10 kpc).

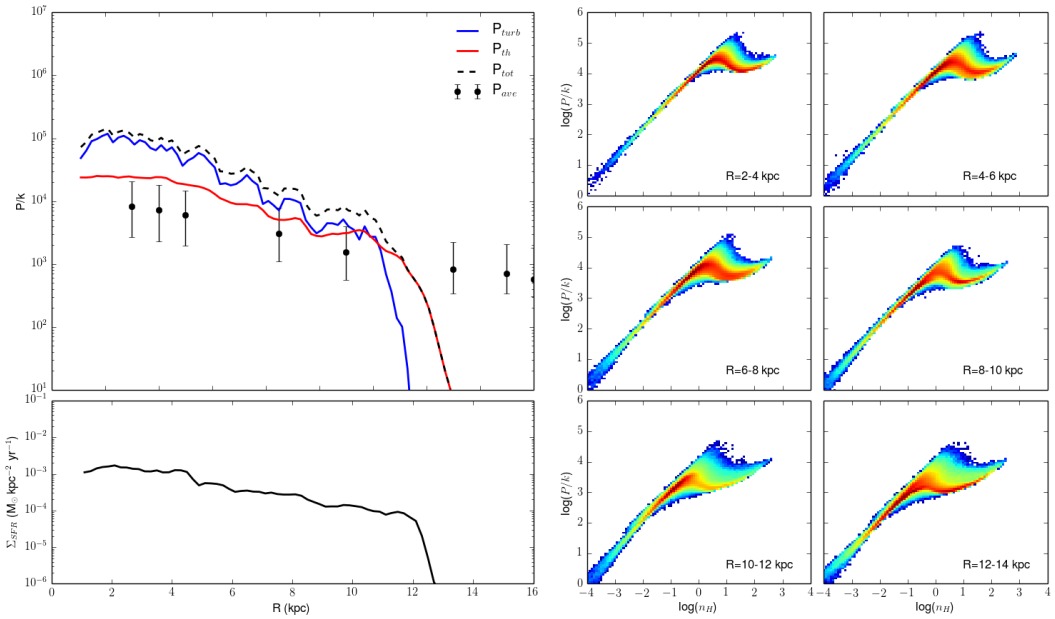

Figure 3.25 ($\Sigma_0 = 14$ M$_\odot$ pc^{-2}) Total, thermal and turbulent pressure averaged for rings through the xy-plane of the disc. Points represent the average thermal pressure required produce a two phase medium (Wolfire et al., 2003). This is compared to phase diagrams for the disc at various radii. In this case star formation continues until the edge of the disc is encountered.

To confirm this behaviour we have completed the same analysis for a higher surface density disc. Figure 3.25 shows the same analysis described above, this time for simulation s14.n100.c1.5. In this case the star formation in the disc is not truncated until approximately 13 kpc. Unfortunately, this corresponds to the edge of the disc; as discussed in Section 2.3.1 the density profile of the initial condition is truncated between the radii of 12 and 14 kpc. What is promising, is that star formation continues to the outer edge of the disc and so does the prevalence of the two-phase instability.

Examining these two cases, and others not shown here, we have seen that large-scale star formation is no longer possible when the ISM loses its ability to separate into distinct warm and cold phases. This is consistent with the findings of Elmegreen & Parravano (1994) and Gerritsen & Icke (1997) that the existence of two ISM phases in thermal pressure equilibrium is crucial to star formation. This is also consistent with the analytic modelling of Schaye (2004), who finds that the truncation of star formation in outer discs corresponds to the disappearance of two-phase structure.

3.3.1 Extended Disc Models

To confirm that the behaviour we see is not an artifact of gas encountering the edges of the disc, we have constructed an extended disc model as described in Section 2.3.1. Figure 3.26 shows face and edge-on density slices for this disc. For this simulation we choose a high star formation density threshold of 10^4 cm^{-3} and decrease the feedback efficiency to 10%. In this simulation the high density ring features are very prominent and very regular. We speculate that in a perturbed galaxy or one with an active potential associated with old stars, these rings would constitute spiral arms. Our simulated galaxies contain no old stellar component, which would lower the effective Q parameter in the disc. If the effective Q parameter in the disc is artificially high, this would suppress the creation of spiral modes due to gravitational instability.

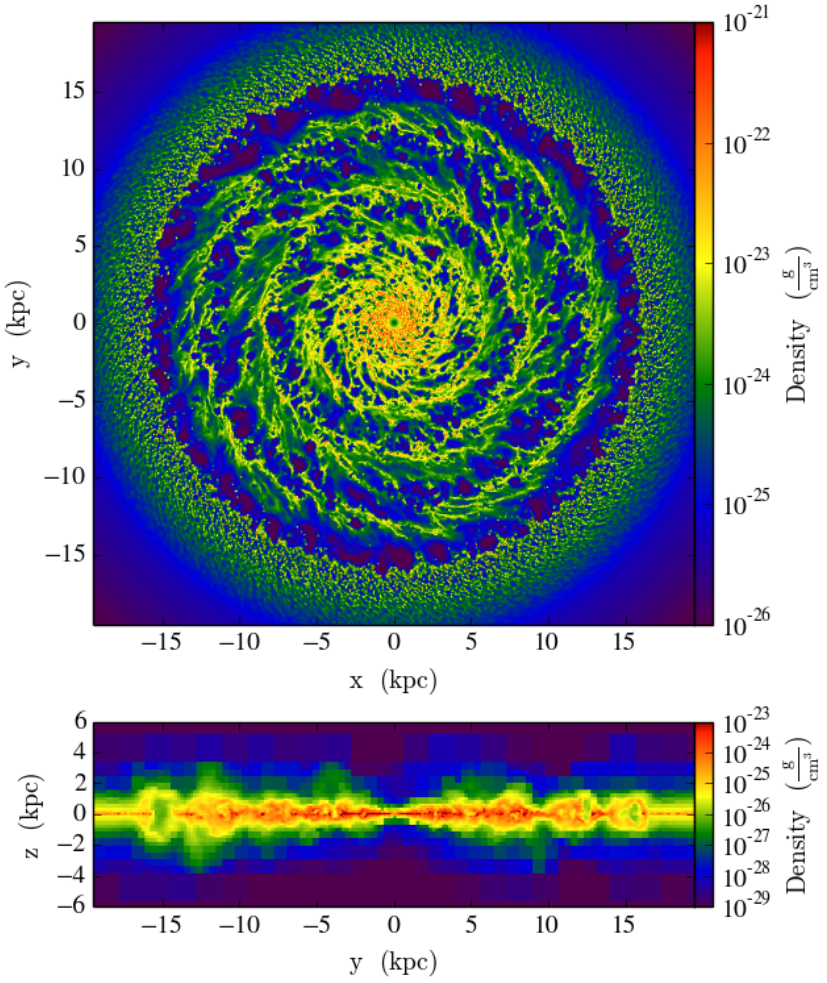

Figure 3.26 Density slice for the fiducial extended disc (s14.n10^4.c5.lowFB.x) at 400 Myr

We take this opportunity to explore the impact of our choice of functional form for the FUV heating term. We experiment by choosing a constant FUV heating rate, clamped to the expected rate for the solar neighbourhood. Again, simulation is done with a high star formation density threshold of 10^4 cm^{-3} and low feedback efficiency (10%). Figure 3.27 shows face and edge-on density

slices for this disc. This constant heating term obliterates any structure outside a galactic radius of $\sim$ 10 kpc.

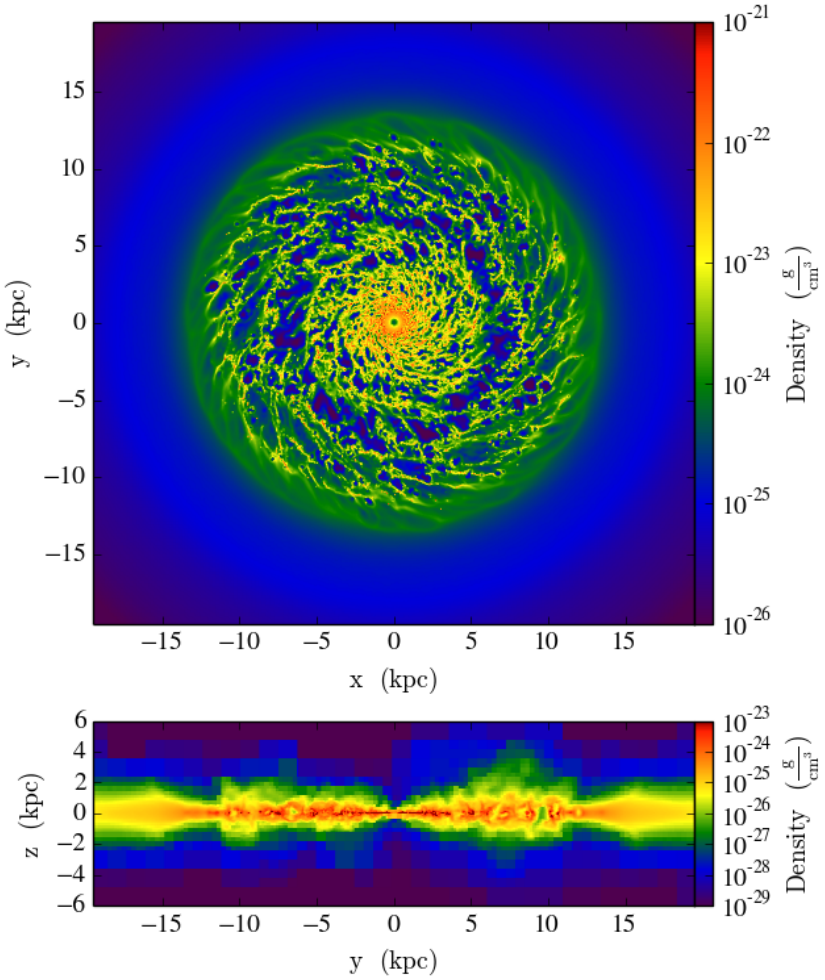

Figure 3.27 Density slice for the an extended disc case (s14.n10^4.c5.lowFB.x.FUVR$_0$) at 400 Myr. This has the FUV heating term set to a constant value equivalent to the typical heating rate at the solar radius, R_0.

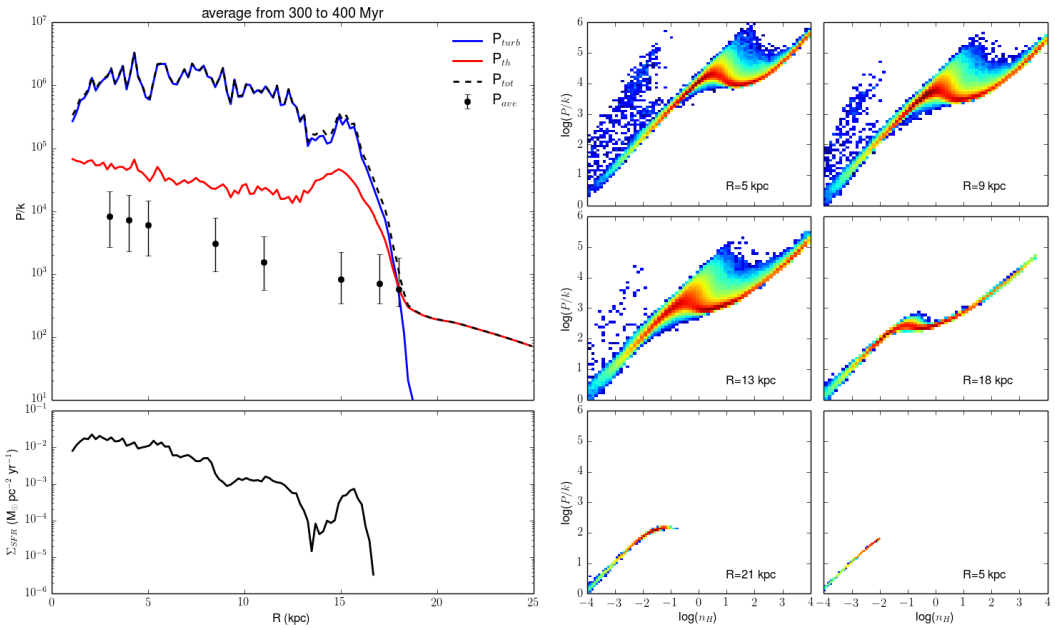

Figure 3.28 Total, thermal and turbulent pressure averaged for rings through the xy-plane of the fiducial extended disc (see Figure 3.26). Points represent the average thermal pressure required produce a two phase medium (Wolfire et al., 2003). This is compared to phase diagrams for the disc at various radii. The truncation of star formation corresponds to the radius in the disc where a two phase medium is no longer sustainable.

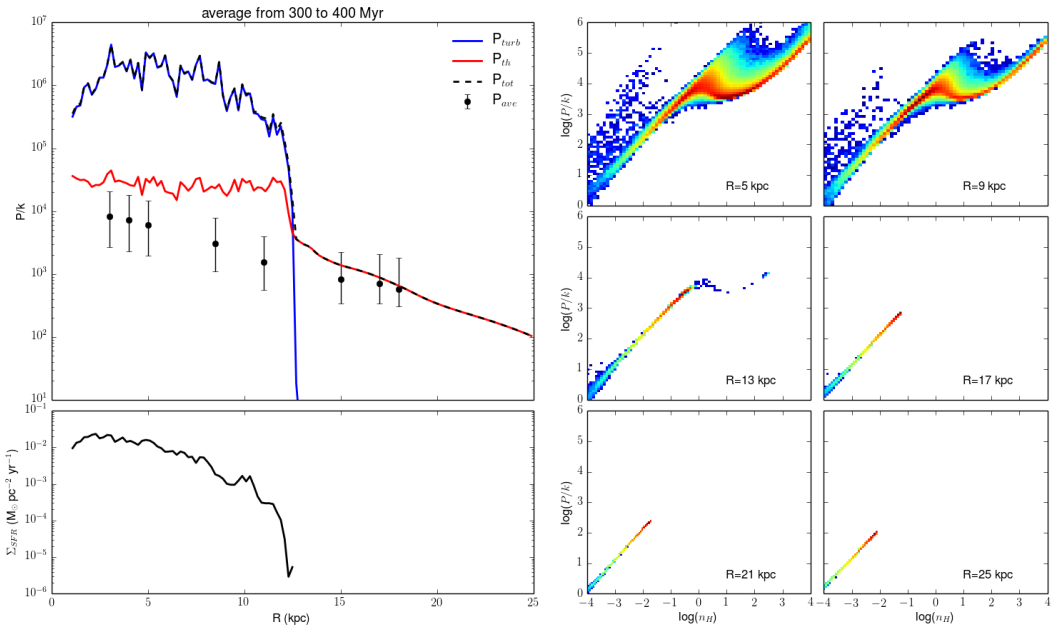

Figure 3.29 Total, thermal and turbulent pressure averaged for rings through the xy-plane of the extended disc with modified FUV heating (see Figure 3.27). Points represent the average thermal pressure required produce a two phase medium (Wolfire et al., 2003). This is compared to phase diagrams for the disc at various radii. The truncation of star formation corresponds to the radius in the disc where a two phase medium is no longer sustainable.

In Figures 3.28 and 3.29 we show the radial pressure and phase diagrams (as in Figures 3.24 and 3.25). In both of these cases the effective pressure is dominated by pressure from turbulence. We see that in the disc with a constant FUV field, star formation truncates much earlier in the disc, at ∼13 kpc as opposed to ∼20 kpc in the disc with a radially varying FUV field. Both discs have been evolved long enough that they have completed one full rotation at a radius of 15 kpc. These cases support our earlier results. The radius at

which star formation dies off is consistent with the radius at which a two phase medium can no longer be sustained. Beyond this radius only a warm phase exists, and this phase is not suitable to host the large scale formation of stars. Isolated events of star formation can still occur locally, where the surface density is high enough.

Bibliography

Elmegreen, B. G. & Parravano, A. 1994, ApJ, 435, L121

Gerritsen, J. P. E. & Icke, V. 1997, A&A, 325, 972

Hopkins, P. F., Quataert, E., & Murray, N. 2011, MNRAS, 417, 950

Kennicutt, R. C. & Evans, N. J. 2012, ARA&A, 50, 531

Kennicutt, Jr., R. C. 1998, ApJ, 498, 541

Krumholz, M. R. & Tan, J. C. 2007, ApJ, 654, 304

Lada, C. J., Lombardi, M., & Alves, J. F. 2010, ApJ, 724, 687

Schaye, J. 2004, ApJ, 609, 667

Tielens, A. G. G. M. 2005, The Physics and Chemistry of the Interstellar Medium

Turk, M. J., Smith, B. D., Oishi, J. S., Skory, S., Skillman, S. W., Abel, T., & Norman, M. L. 2011, ApJS, 192, 9

Wolfire, M. G., McKee, C. F., Hollenbach, D., & Tielens, A. G. G. M. 2003, ApJ, 587, 278

Wyder, T. K., Martin, D. C., Barlow, T. A., Foster, K., Friedman, P. G., Morrissey, P., Neff, S. G., Neill, J. D., Schiminovich, D., Seibert, M., Bianchi,

L., Donas, J., Heckman, T. M., Lee, Y.-W., Madore, B. F., Milliard, B., Rich, R. M., Szalay, A. S., & Yi, S. K. 2009, ApJ, 696, 1834

Chapter 4

Conclusions & Future Work

We have run a suite of high resolution simulations of isolated galaxies. We have used this suite to study the impacts of numerical recipe parameters on the resulting galaxies. Varying the density threshold for star formation, $n_{\rm th}$, and the star formation efficiency, c_* have little effect on the global star formation rate of the simulated galaxies. These parameters do, however, change the structure of the ISM. Increasing $n_{\rm th}$ forces star formation to proceed in a more clustered mode. This clustered mode of star formation allows more dense/cold gas to survive. Increasing c_* by an order of magnitude will increase the global star formation rate by a factor of three. This increase in the amount of stars, increases the total effective pressure in the disk. This leads to cases with large efficiency having larger gas scale heights.

Varying parameters related to the stellar feedback have varying impacts on the simulated galaxies. In high surface density cases, decreasing $\epsilon_{\rm FB}$ by an order of magnitude is accompanied by an order of magnitude increase in the global star formation rate. This change corresponds to a decrease in the fraction of cold gas and an increase in the cold gas scale height. In our low surface density disks, the total pressure is dominated by the thermal pressure set by

the photoelectric heating term. In these cases, varying feedback parameters have little impact on the star formation rate and the ISM.

We have used a sub-sample of our simulation suite to explore the truncation of star formation in the outer regions of galactic disks. Our findings are consistent with those of Schaye (2004). We find that the truncation of star formation corresponds to radii in the disk where a two-phase thermal instability can no longer be sustained.

Our results might be different if we had a self-consistent treatment for the FUV heating. This heating term should correlate with star formation, which is not the case in our current model. A full treatment of radiative transfer has newly been incorporated into GASOLINE (Woods et al., in prep.). We plan to run simulations using this new treatment. Our chosen feedback algorithm is very effective at heating gas (almost too effective). Supernovae are able to blow large holes in the disks and may be responsible for creating the strong high density ring features. It would be instructive to redo a selection of simulations with low feedback efficiency or using the new super-bubble feedback model of Keller et al. (2014).

In simulations higher resolution is always desired. We were only able to complete two ultra-high resolution simulations ($m_p = 55.24$ M$_\odot$) due to time constraints. Results from chapter 3 suggest that while the star formation rate is converged, quantities like the fraction of cold gas are affected by resolution; the higher the resolution the higher the fraction of surviving cold gas. We have plans to re-simulate disk sections at higher resolution. This will allow us to directly study the structure of individual star-forming GMCs.

Bibliography

Keller, B. W., Wadsley, J., Benincasa, S. M., & Couchman, H. M. P. 2014, MNRAS, 442, 3013

Schaye, J. 2004, ApJ, 609, 667

This page intentionally left blank.